

Estimating Uncertainty in Neural Networks for Cardiac MRI Segmentation: A Benchmark Study

Matthew Ng^{a,b,*}, Fumin Guo^{a,b}, Labonny Biswas^a, Steffen E. Petersen^{c,d}, Stefan K. Piechnik^e, Stefan Neubauer^e, Graham Wright^{a,b}

^aPhysical Sciences Platform, Sunnybrook Research Institute, Toronto, ON, Canada

^bDepartment of Medical Biophysics, University of Toronto, Toronto, ON, Canada

^cWilliam Harvey Research Institute, NIHR Barts Biomedical Research Centre, Queen Mary University of London, UK

^dBarts Heart Centre, St Bartholomew's Hospital, Barts Health NHS Trust, West Smithfield, London, UK

^eDivision of Cardiovascular Medicine, Oxford NIHR Biomedical Research Centre, Radcliffe Department of Medicine, University of Oxford, Oxford, UK

Abstract

Convolutional neural networks (CNNs) have demonstrated promise in automated cardiac magnetic resonance imaging segmentation. However, when using CNNs in a large real-world dataset, it is important to quantify segmentation uncertainty in order to know which segmentations could be problematic. In this work, we performed a systematic study of Bayesian and non-Bayesian methods for estimating uncertainty in segmentation neural networks. We evaluated Bayes by Backprop (BBB), Monte Carlo (MC) Dropout, and Deep Ensembles in terms of segmentation accuracy, probability calibration, uncertainty on out-of-distribution images, and segmentation quality control. We tested these algorithms on datasets with various distortions and observed that Deep Ensembles outperformed the other methods except for images with heavy noise distortions. For segmentation quality control, we showed that segmentation uncertainty is correlated with segmentation accuracy. With the incorporation of uncertainty estimates, we were able to reduce the percentage of poor segmentation to 5% by flagging 31% to 48% of the most uncertain images for manual review, substantially lower than random review of the results without using neural network uncertainty.

Keywords: Cardiac MRI segmentation, segmentation quality control, Bayesian neural networks, uncertainty

1. Introduction

Cardiac magnetic resonance imaging (MRI) is the gold standard for evaluating cardiac function due to its excellent soft tissue contrast, high spatial and temporal resolution, and non-ionizing radiation (Peng et al., 2016). Segmentation of cardiac structures such as the left ventricle cavity, left ventricle myocardium, and right ventricle cavity is required as a first step to quantify clinically relevant imaging biomarkers such as the left ventricle ejection fraction and myocardial mass. Recently, convolutional neural networks (CNNs) have been shown to perform well for automatic cardiac MR image segmentation (Bai et al., 2018; Bernard et al., 2018). However, when using a CNN in an automated image analysis pipeline, it is important to know which segmentation results are problematic and require further manual inspection. This may improve workflow efficiency by focusing on problematic segmentations, avoiding the review of all images and reducing errors in downstream analysis.

This problem has been referred to as *segmentation quality control*, and is closely related to the task of anomaly detection or out-of-distribution detection (Bishop, 1994). One approach to solve this problem is to use predictive uncertainty estimates of a segmentation model. The key idea here is that segmentation outputs with low uncertainty are *likely* correct while outputs

with high uncertainty are *likely* problematic. While several studies have attempted to estimate uncertainty in CNNs for medical image segmentation, most of these studies used Monte Carlo (MC) Dropout or Deep Ensembles. However, there are some limitations associated with these methods, which motivates exploration of other algorithms for estimating uncertainty. For example, when using a fixed dropout rate in MC Dropout, the model uncertainty does not decrease as more training data is used. This is potentially problematic since model uncertainty should approach zero in the limit of infinite data (Osband, 2016). As a result, the dropout rate needs to be tuned depending on the model size and amount of training data (Gal, 2016). For Deep Ensembles, it is not clear *why* this method generates well-calibrated uncertainty estimates. In addition, in previous studies, evaluation of these algorithms was mostly limited to correlations between the predictive uncertainty and segmentation accuracy or metrics measuring how uncertainty can be used to improve segmentation (Roy et al., 2018; Jungo et al., 2018; Sander et al., 2019). In this work, we compared Bayesian and non-Bayesian approaches and performed a systematic evaluation of epistemic uncertainty for these methods. In particular, we evaluated Bayes by Backprop (BBB), MC Dropout, and Deep Ensembles based on segmentation accuracy, probability calibration, uncertainty on out-of-distribution datasets, and finally, demonstrated the utility of these methods for segmentation quality control.

*Corresponding author: 2075 Bayview Avenue, Toronto, ON M4N 3M5.
Email: matthewng.ng@mail.utoronto.ca (Matthew Ng)

1.1. Uncertainty in Neural Networks

Uncertainty in neural networks can be estimated using Bayesian and non-Bayesian methods. Bayesian neural networks (BNNs) provide a theoretical framework for generating well-calibrated uncertainty estimates (Neal, 2012). In BNNs, we are interested in learning the posterior distribution of the neural network weights instead of a maximum likelihood or maximum-a-posteriori estimate. A challenge in learning BNNs is that integrating over the posterior is intractable in high dimensional space. As such, approximate inference techniques such as stochastic variational inference are commonly used. Examples include variational dropout (Kingma et al., 2015), MC dropout (Gal and Ghahramani, 2016), Bayes by Backprop (Blundell et al., 2015), multiplicative normalizing flows (Louizos and Welling, 2017), and Flipout (Wen et al., 2018).

Non-Bayesian methods can also be used to estimate uncertainty in neural networks. Examples include bootstrapping (Efron and Tibshirani, 1986), Deep Ensembles (Lakshminarayanan et al., 2017), Temperature Scaling (Guo et al., 2017), and Resampling Uncertainty Estimation (Schulam and Saria, 2019). Note that in Bayesian methods, uncertainty is learned during training and is tightly coupled to the model structure. In non-Bayesian methods, uncertainty is learned during training or estimated after training.

In this work, we focused on modelling epistemic uncertainty using Bayesian and non-Bayesian methods. Epistemic or model-based uncertainty is uncertainty related to model parameters due to the use of a finite amount of training data. For humans, epistemic uncertainty corresponds to uncertainty from inexperienced or non-expert observers. In contrast, aleatoric or data-dependent uncertainty is related to the data itself and corresponds to inter- and intra-observer variability. Epistemic uncertainty is more applicable for segmentation quality control since segmentation outputs with high aleatoric uncertainty may be considered acceptable from a quality control perspective as long as the output matches the expectations from one or more experienced observers.

1.2. Related Studies

Bayesian neural networks have been used for medical image segmentation tasks; however, most work used MC Dropout to approximate the posterior distribution of the weights and investigations of ways to evaluate the quality of uncertainty have been limited. Roy et al. (2018), Jungo et al. (2018), and Wang et al. (2019b) used a CNN with MC Dropout for brain structure, brain tumour, and brain tumour cavity segmentation. These studies observed positive correlations between segmentation accuracy and uncertainty measures. Nair et al. (2019) compared different uncertainty measures in brain lesion segmentation and showed that uncertainty measures can be used to improve lesion detection accuracy. Sander et al. (2019) applied MC Dropout on a CNN for cardiac MRI segmentation and showed that training using a Brier loss or cross-entropy loss produced well-calibrated pixel-wise uncertainties, and correcting uncertain pixels can improve segmentation results consistently. DeVries and Taylor (2018) used MC Dropout and other non-Bayesian methods

to generate skin lesion segmentation and the segmentation uncertainty maps, which were then entered into another neural network to predict the Jaccard index of the segmentation. Hann et al. (2019) proposed segmentation quality estimates for aortic MRI segmentation using an ensemble of neural networks and demonstrated improved segmentation accuracy with the use of these estimates. More recently, Jungo and Reyes (2019) compared MC Dropout, Deep Ensembles, and auxiliary networks for predicting pixel-wise segmentation errors for two medical image segmentation tasks. In addition to segmentation probability calibration, they examined the overlap between segmentation uncertainty and errors, and the fraction of images which would benefit from uncertainty-guided segmentation correction. In a follow-up work, Jungo et al. (2020) compared different aggregation methods for uncertainty measures and their performance for segmentation failure detection. Similarly, Mehrtash et al. (2020) also compared MC Dropout and Deep Ensembles for CNNs trained with different loss functions in terms of probability calibration and correlation between segmentation accuracy and uncertainty measures. However, these studies did not evaluate other Bayesian methods such as Bayes by Backprop for uncertainty estimation and the performance of these methods on out-of-distribution datasets is unknown. In this work, we evaluated and compared several commonly used uncertainty estimation methods on datasets with various degrees of distortions, which mimic the clinical scenarios. We analyzed the strengths and limitations of these methods on datasets with various distortions, and finally, demonstrated the utility of these algorithms for segmentation quality control.

1.3. Contributions

While MC Dropout and Deep Ensembles have been used to estimate uncertainty in medical image segmentation, limited studies have investigated other Bayesian methods and a comparison of these methods is currently lacking. To this end, we performed a systematic study of Bayesian and non-Bayesian neural networks for estimating uncertainty in the context of cardiac MRI segmentation. Our contributions are listed as follows:

1. We compared MC Dropout and Deep Ensembles with Bayes by Backprop (BBB), which is a more theoretically justified algorithm for learning uncertainty in Bayesian neural networks. We performed a comprehensive evaluation of these algorithms in terms of segmentation accuracy, probability calibration, uncertainty on out-of-distribution datasets, and segmentation quality control.
2. We tested MC Dropout, Deep Ensembles, and BBB on cardiac MRI datasets with various degrees of noise, blurring, and stretching distortions to mimic complex clinical scenarios and to investigate the relationships between image distortions and neural network uncertainty estimates. We showed that BBB is more robust to noise distortions while Deep Ensembles is more resistant to blurring and stretching distortions used in this study.
3. We introduced a novel area-under-the-curve metric for quantifying algorithm performance on segmentation quality control. We showed that with the use of Deep Ensembles

uncertainty estimates, only 31% to 48% of the most uncertain segmentations need to be reviewed to reduce the percentage of poor segmentations to 5%, whereas ~80% of the images need to be reviewed when neural network uncertainty measures are not used.

We hope this work will serve as a benchmark for evaluating uncertainty in cardiac MRI segmentation and inspire further work on uncertainty estimation in medical image segmentation.

2. Methods

2.1. Bayesian Neural Networks (BNN)

Given a dataset of N images $\mathbf{X} = \{\mathbf{x}_i\}_{i=1\dots N}$ and the corresponding segmentation $\mathbf{Y} = \{\mathbf{y}_i\}_{i=1\dots N}$ with C classes, we fit a neural network parameterized by weights \mathbf{w} to perform segmentation. In BNNs, we are interested in learning the posterior distribution of the weights, $p(\mathbf{w}|\mathbf{X}, \mathbf{Y})$, instead of a maximum likelihood or maximum-a-posteriori estimate. This posterior distribution represents uncertainty in the weights, which could be propagated to calculate uncertainty in the predictions (MacKay, 1995). In addition, BNNs have been shown to be able to improve the generalizability of neural networks (MacKay, 1995).

A challenge in learning BNNs is that calculating the posterior is intractable due to its high dimensionality. Variational inference (Hoffman et al., 2013) is a scalable technique that aims to learn an approximate posterior distribution of the weights $q(\mathbf{w})$ by minimizing the Kullback-Leibler (KL) divergence between the approximate and true posterior. This is equivalent to maximizing the evidence lower bound (ELBO) as follows:

$$q(\mathbf{w}) = \arg \max_{q(\mathbf{w})} \mathbb{E}_{q(\mathbf{w})}[\log p(\mathbf{Y}|\mathbf{X}, \mathbf{w})] - \lambda \cdot \text{KL}[q(\mathbf{w})||p(\mathbf{w})], \quad (1)$$

where $\mathbb{E}_{q(\mathbf{w})}[\cdot]$ denotes expectation over the approximate posterior $q(\mathbf{w})$, $\log p(\mathbf{Y}|\mathbf{X}, \mathbf{w})$ is the log-likelihood of the training data with given weights \mathbf{w} , $p(\mathbf{w})$ represents the prior distribution of \mathbf{w} , and $\text{KL}[\cdot]$ is the Kulback-Leibler divergence between two probability distributions weighted by a hyperparameter $\lambda > 0$ to achieve better performance.

State-of-the-art segmentation neural networks such as the U-net formulate image segmentation as pixelwise classification. For each pixel $x_{i,j}$ in image \mathbf{x}_i , $i = 1, \dots, N$, $j \in \Omega$, the neural network generates a prediction $\hat{y}_{i,j}$ with probability $p(\hat{y}_{i,j} = c)$, $c = 0, 1, \dots, C - 1$, through softmax activation of the features in the last layer. Assuming each pixel is independent from other pixels in the image, the log likelihood of the training data in Eq. (1) is given by:

$$\log p(\mathbf{Y}|\mathbf{X}, \mathbf{w}) = \sum_{i=1}^N \sum_{j \in \Omega} \sum_{c=0}^{C-1} [y_{i,j} = c] \cdot \log p(\hat{y}_{i,j} = c),$$

where $y_{i,j}$ is the ground truth label for pixel j in the i^{th} image, and $[\cdot]$ is the indicator function. In this setting, the log likelihood is the same as the negative cross entropy between the ground truth and predicted segmentation. The prediction $\hat{\mathbf{y}}$ of the BNN

on a test image \mathbf{x} is generated by marginalizing out the weights of the neural network, i.e.,

$$p(\hat{\mathbf{y}}|\mathbf{x}) = \mathbb{E}_{q(\mathbf{w})}[p(\hat{\mathbf{y}}|\mathbf{x}, \mathbf{w})], \quad (2)$$

where $p(\hat{\mathbf{y}}|\mathbf{x}, \mathbf{w})$ denotes the prediction given a set of weights \mathbf{w} . In the next two sections, we introduce methods for estimating an approximate posterior $q(\mathbf{w})$ for the weights of a neural network.

2.1.1. Bayes by Backprop

One way to parameterize the approximate posterior $q(\mathbf{w})$ is to use a fully factorized Gaussian. This is sometimes called mean-field variational inference. In a fully factorized Gaussian, each weight w in \mathbf{w} is independent from other weights and follows a Gaussian distribution with mean μ and standard deviation σ . To ensure $\sigma > 0$ and training stability, σ is parameterized by a real number ρ , i.e., $\sigma = \text{softplus}(\rho) = \ln(1 + e^\rho)$. The prior distribution $p(\mathbf{w})$ is usually chosen as a fully factorized Gaussian with mean $\mu_{\text{prior}}\mathbf{I}$ and standard deviation $\sigma_{\text{prior}}\mathbf{I}$, i.e., $p(\mathbf{w}) = \mathcal{N}(\mu_{\text{prior}}\mathbf{I}, \sigma_{\text{prior}}\mathbf{I})$, where \mathbf{I} represents the identity matrix. Gradient updates can be performed using the ‘‘reparameterization trick’’. The training procedure is known as Bayes by Backprop (BBB) (Blundell et al., 2015) and described below:

1. For each weight w , sample $\epsilon \sim \mathcal{N}(0, 1)$ and set $w = \mu + \text{softplus}(\rho) \circ \epsilon$.
2. Calculate the loss function \mathcal{L} based on Eq. (1), i.e., $\mathcal{L} = -\log p(\mathbf{Y}|\mathbf{X}, \mathbf{w}) + \lambda \cdot \text{KL}[q(\mathbf{w})||\mathcal{N}(\mu_{\text{prior}}\mathbf{I}, \sigma_{\text{prior}}\mathbf{I})]$.
3. Update μ and ρ through gradient descent.

After training, each weight can be sampled from $\mathcal{N}(\mu, \sigma)$, which is then used to generate the predicted segmentation using Eq. (2).

2.1.2. MC Dropout

MC Dropout (MCD) (Gal and Ghahramani, 2016) is another commonly used method for learning BNNs because it is straightforward to implement and does not require additional parameters or weights. MCD can be interpreted as choosing the approximate posterior distribution $q(\mathbf{w})$ to be a mixture of two Gaussians with minimal variances, e.g., one at 0 and the other at the weight w . Dropout is applied during training and testing to sample weights from $q(\mathbf{w})$. In this method, the dropout rate is a hyperparameter chosen empirically based on a validation dataset. The dropout rate defines the amount of uncertainty in the weights and is fixed throughout network training and testing.

2.2. Deep Ensembles

In addition to BNNs, we characterized and evaluated uncertainty estimates using an ensemble of neural networks. This is also known as Deep Ensembles (Lakshminarayanan et al., 2017). Deep Ensembles consist of multiple neural networks trained using the same data (or different subsets of the same data) with different random initializations. Combination of the models in an ensemble has been shown to produce well-calibrated probabilities in computer vision tasks, and the variability in the models can be used to calculate predictive uncertainty. This non-Bayesian approach was inspired by the idea of bootstrapping,

where stochasticity in the sampling of the training data and training algorithm define model uncertainty. This approach differs from Bayesian methods since it does not require approximation of the posterior distribution of the weights.

2.3. Algorithm Evaluation

We evaluated the uncertainty estimation algorithms based on three aspects: (1) segmentation accuracy and probability calibration, (2) uncertainty on out-of-distribution images, and (3) application of uncertainty estimates for segmentation quality control. The purposes of these evaluations are as follows:

(1) We show that Bayesian neural networks can provide segmentation accuracies that are similar or higher than plain or point estimate neural networks. In addition, predicted segmentation probabilities should be well-calibrated, i.e., a pixel with a predicted probability of 60% belonging to the myocardium is truly 60%. From a frequentist perspective, this means that out of all predictions with 60% probability, 60% of the predictions are correct.

(2) We measure segmentation uncertainty on out-of-distribution images to validate that the uncertainty measures perform as expected, i.e., uncertainty should increase when test images are substantially different from training datasets.

(3) We expect uncertainty measures to be useful in identifying problematic segmentations that require manual editing.

We first discuss metrics for segmentation accuracy and probability calibration and then present methods to quantify predictive uncertainty using uncertainty measures.

2.3.1. Segmentation Accuracy

Let R_a and R_m be the automated and manual segmentation regions, respectively. We calculated the algorithm segmentation accuracy using Dice similarity coefficient, average symmetric surface distance (ASSD), and Hausdorff distance (HD).

Dice measures the overlap between two segmentations and is given by:

$$\text{Dice} = \frac{2|R_a \cap R_m|}{|R_a| + |R_m|}.$$

ASSD quantifies the average distance between the contours of two segmentation regions and is given by:

$$\text{ASSD} = \frac{1}{2|\partial R_a|} \sum_{p \in \partial R_a} d(p, \partial R_m) + \frac{1}{2|\partial R_m|} \sum_{p \in \partial R_m} d(p, \partial R_a),$$

where $|\partial R_a|$ represents the number of points on contour ∂R_a and $d(p, \partial R_m)$ represents the shortest Euclidean distance from point p to contour ∂R_m ; $|\partial R_m|$ and $d(p, \partial R_a)$ are defined in the same manner.

HD is the maximum distance between two contours and is calculated as:

$$\text{HD} = \max(\max_{p \in \partial R_a} d(p, \partial R_m), \max_{p \in \partial R_m} d(p, \partial R_a)).$$

2.3.2. Probability Calibration

These metrics measure how closely the neural network segmentation probabilities match the ground truth probabilities generated from manual segmentation on a per-pixel basis.

Following the notation in Sec. 2.1, we let \hat{y}_j and y_j denote the prediction and ground truth label of pixel j in a given image, $j \in \Omega$, respectively. **Negative log likelihood (NLL)** measures how well the learned model fits the observed (testing) data. Note that NLL is sensitive to tail probabilities; that is, a model that generates low probability for the correct class is heavily penalized. NLL is calculated as:

$$\text{NLL} = \sum_{j \in \Omega} \sum_{c=0}^{C-1} [y_j = c] \cdot \log p(\hat{y}_j = c).$$

Brier score (BS) measures the mean squared error between the predicted and ground truth probabilities and is given by:

$$\text{BS} = \sum_{j \in \Omega} \sum_{c=0}^{C-1} [p(\hat{y}_j = c) - p(y_j = c)]^2.$$

2.3.3. Predictive Uncertainty Measures

Predictive uncertainty measures can be calculated from the neural network predictions to indicate the degree of certainty of the output. These can be calculated per pixel or per structure/class.

Pixelwise Uncertainty Measures. Pixelwise uncertainty measures are motivated by information theory. These values are calculated per pixel and averaged across all pixels in the image if an image-level measure is required. In this work, we used the following pixelwise uncertainty measures:

- **Predictive Entropy** measures the spread of probabilities across all the classes in the mean prediction and is given by:

$$\sum_{j \in \Omega} \sum_{c=0}^{C-1} [-p(\hat{y}_j = c) \log p(\hat{y}_j = c)].$$

- **Mutual Information (MI)** measures how different each sample is from the mean prediction and is calculated as:

$$\mathbb{E}_{q(\mathbf{w})} \left[\sum_{j \in \Omega} \sum_{c=0}^{C-1} p(\hat{y}_j = c | \mathbf{w}) \log p(\hat{y}_j = c | \mathbf{w}) - \sum_{j \in \Omega} \sum_{c=0}^{C-1} p(\hat{y}_j = c) \log p(\hat{y}_j = c) \right],$$

where $p(\hat{y}_j = c | \mathbf{w})$ denotes the prediction given a set of weights \mathbf{w} . MI is high if there are samples with both high and low confidence, and is low if all samples have low confidence or high confidence.

Structural uncertainty measures. Structural uncertainty measures were proposed specifically for image segmentation (Roy et al., 2018). Here, we define two structural uncertainty measures, which quantify how different each structure is among the prediction samples in terms of Dice and ASSD. We expect structural uncertainty measures to better align with common segmentation accuracy metrics because of their focus on global image-level uncertainty.

- $\text{Dice}_{\text{WithinSamples}} = \frac{1}{T} \sum_{i=1}^T \text{Dice}(\bar{S}, S_i)$
- $\text{ASSD}_{\text{WithinSamples}} = \frac{1}{T} \sum_{i=1}^T \text{ASSD}(\bar{S}, S_i)$

where \bar{S} is the mean predicted segmentation and $S_i, i \in \{1 \dots T\}$, are individual prediction samples from the neural network.

2.4. Datasets

2.4.1. UK BioBank (UKBB)

The UKBB dataset (Petersen et al., 2015) consists of images from 4845 healthy volunteers. For each subject, 2D cine cardiac MR images were acquired on a 1.5T Siemens scanner using a bSSFP sequence under breath-hold conditions with ECG-gating (pixel size = 1.8-2.3 mm, slice thickness = 8 mm, number of slices = ~ 10 , number of phases = ~ 50). Manual segmentation of the left ventricle blood pool (LV), left ventricle myocardium (Myo), and right ventricle (RV) was performed on the end-diastolic (ED) and end-systolic (ES) phases by one of eight observers followed by random checks by an expert to ensure segmentation quality and consistency. The dataset was randomly split into 4173, 103, and 569 subjects for training, validation, and testing, respectively. These numbers were chosen for convenience.

2.4.2. Automated Cardiac Diagnosis Challenge (ACDC)

The ACDC dataset (Bernard et al., 2018) consists of 100 patients with one of five conditions: normal, myocardial infarction, dilated cardiomyopathy, hypertrophic cardiomyopathy, and abnormal right ventricle. 2D Cine MR images were acquired using a bSSFP sequence on a 1.5T/3T Siemens scanner (pixel size = 0.7-1.9 mm, slice thickness = 5-10 mm, number of slices = 6-18, number of phases = 28-40). Manual segmentation was performed at the ED and ES phases with approval by two experts. This dataset was used for testing only.

2.5. Training Details

We used a plain 2D U-net (Ronneberger et al., 2015) for MC Dropout, BBB, and Deep Ensembles. The plain U-net consisted of 10 layers with 3×3 filters and 2 layers with 1×1 convolutions followed by a softmax layer. The number of filters ranged from 32 to 512 from the top to the bottom layers.

For MCD, we added dropout on all layers or only on the middle layers of the U-net with different dropout rates: 0.5, 0.3, 0.1. These settings effectively tuned the amount of uncertainty in the model. For BBB, we experimented with different standard deviations of the prior distributions: $\sigma_{\text{prior}} = 0.1$ or 1.0 and different weights for the KL term: $\lambda = 0.1, 1.0, 10, 30$. These are commonly used hyperparameters in the literature (Kendall

et al., 2017; Blundell et al., 2015; Fortunato et al., 2017). For both methods, the final prediction was obtained by averaging the softmax probabilities of 50 samples. For Deep Ensembles, we trained 10 plain U-net models separately using all of the training data with different random initializations and averaged the softmax probabilities of the 10 models. For each method, we saved models with the lowest NLL on the validation dataset since NLL is directly related to segmentation accuracy and probability calibration.

For preprocessing, the input images were cropped by taking a region of 160x160 pixels from the center of the original images. Then, image intensities were normalized by subtracting the mean and dividing by the variance of the entire training dataset. Experiments were repeated 5 times (except for Deep Ensembles) and the results were averaged. Data augmentation was performed, including random rotation (-60 to 60 degrees), translation (-60 to 60 pixels), and scaling (0.7 to 1.3 times). These models were trained using the Adam optimizer for 50 epochs. The initial learning rate was set to 1e-4 which was decayed to 1e-5 after 30 epochs.

3. Experiments and Results

For BBB, $\lambda = 10$ and $\sigma_{\text{prior}} = 0.1$ achieved the best validation negative log likelihood. For MC Dropout, adding dropout on the middle layers with a dropout rate of 0.1 (MCD-0.1) performed the best. We also reported results for MC Dropout with a dropout rate of 0.5 on the middle layers (MCD-0.5) for comparison since this setting is commonly used in the literature.

3.1. Segmentation Accuracy and Probability Calibration

The segmentation accuracy and probability calibration of the U-net trained with various methods are shown in Table 1. Deep Ensembles performed the best in terms of segmentation accuracy and probability calibration. This was followed by BBB and MCD-0.1, which were comparable to the plain U-net. MCD-0.5 performed slightly worse than other models in terms of segmentation accuracy and probability calibration. These results indicate that Bayesian approaches or Deep Ensembles can yield similar, if not better, segmentation results compared to a plain U-net while providing uncertainty estimates at the same time.

3.2. Uncertainty on Distorted Images

In order to validate uncertainty measures as indicators of “out-of-distribution” datasets, we applied the trained models to carefully generated images with various magnitudes of distortions, including:

- adding Rician noise, as found in MR images (Gudbjartsson and Patz, 1995), with magnitudes ranging from 0.05 to 0.10 (images intensities ranged from 0 to 1),
- Gaussian blurring with a standard deviation of 1.0 to 4.0 pixels, and
- deforming or stretching around the cardiac structures.

Table 1: Segmentation accuracy (N=1138 images) and probability calibration of the plain U-net, U-net with MC Dropout, BBB, or Deep Ensemble. \uparrow indicates higher is better. \downarrow indicates lower is better. Format: Mean (Standard Deviation).

	Dice \uparrow			ASSD (mm) \downarrow			HD (mm) \downarrow			NLL \downarrow	BS \downarrow
	LV	Myo	RV	LV	Myo	RV	LV	Myo	RV	($\times 10^{-2}$)	($\times 10^{-3}$)
Plain	.941(.038)	.882(.031)	.907(.043)	1.01(.38)	1.02(.43)	1.61(.69)	2.98(0.99)	3.83(1.39)	6.53(2.67)	1.11(.38)	1.67(.54)
BBB	.942(.037)	.883(.030)	.908(.043)	1.00(.36)	1.00(.30)	1.60(.70)	2.96(0.96)	3.80(1.23)	6.39(2.59)	1.10(.35)	1.66(.53)
MCD-0.1	.941(.037)	.882(.030)	.907(.043)	1.00(.36)	1.01(.31)	1.61(.70)	2.97(0.97)	3.82(1.24)	6.49(2.59)	1.10(.36)	1.66(.53)
MCD-0.5	.940(.038)	.879(.030)	.906(.043)	1.03(.38)	1.04(.31)	1.64(.69)	3.05(1.03)	3.95(1.29)	6.64(2.61)	1.13(.35)	1.70(.53)
Ensemble	.943(.037)	.885(.030)	.909(.043)	0.98(.36)	0.98(.29)	1.57(.72)	2.90(0.93)	3.68(1.20)	6.26(2.56)	1.07(.35)	1.63(.52)

Note that these distortions were not applied as part of data augmentation during training and these images were not seen by the neural network. Figure 1 shows examples of the distorted images. We expected decreased segmentation accuracy and increased predictive uncertainty in images with greater magnitudes of distortions.

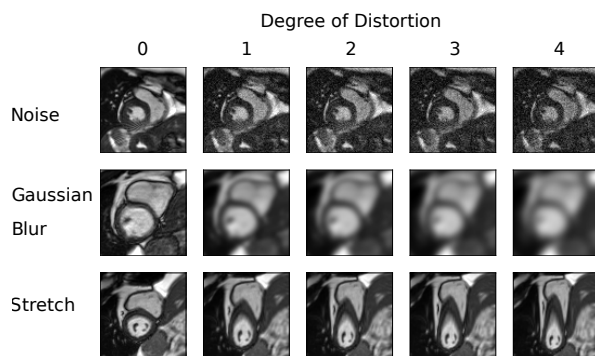


Figure 1: Images with increasing noise (magnitude = [0.05, 0.10]), gaussian blur (standard deviation = [1, 4] pixels), and stretch. These images were generated for systematic evaluation of the algorithms on out-of-distribution datasets. Reproduced by kind permission of UK Biobank \copyright .

3.2.1. Trends with Increasing Distortions

Figure 2 and Supplementary Table 1 show that segmentation accuracy decreased as the magnitude of the distortions (noise, gaussian blur, stretch) was increased. This is expected since these types of distortions were not seen during training and increasing the magnitude of the distortions resulted in greater differences with the original training datasets.

In addition, we observed that the predictive uncertainty increased (i.e., higher predictive entropy, mutual information, $ASSD_{\text{WithinSamples}}$, and lower $Dice_{\text{WithinSamples}}$) with increasing magnitude of distortions but decreased after a certain threshold, as shown in Figure 2. This was the case for Deep Ensembles, BBB, and MC Dropout on images with blurring and noise distortions but not with stretching. For example, for BBB, the median predictive entropy for images with slight, moderate, and large additional noise was 1.66×10^{-2} , 1.95×10^{-2} , and 1.23×10^{-2} , respectively. Similarly, the median $ASSD_{\text{WithinSamples}}$ for the BBB model was 0.40, 3.40, and 0.71 mm for images with slight, moderate, and large amount of blurring, respectively (See Supplementary Table 3 for more details). Figure 3 shows examples of segmentation results and the corresponding predictive entropy and mutual information.

While the increasing predictive uncertainty associated with increasing magnitude of distortions was expected, the decrease in predictive uncertainty after a threshold in cases of noise and blurring distortions was not expected. Specifically, for images that were highly distorted, all pixels were being classified as background with low uncertainty (Figure 2, bottom row). Although this seems correct when only given the labeling choice of background, LV, Myo, and RV, we argue that the distorted pixels are markedly different from the background pixels in the training images and therefore, should have high uncertainty nonetheless. This is a limitation of all the uncertainty models tested and may be improved using more expressive posteriors.

Another observation is that the uncertainty measures began to fail/decrease when dramatic segmentation errors occurred (Figure 2). This suggests that other heuristics or algorithms such as those presented in Ruijsink et al. (2019) can be used to complement the uncertainty measures when trying to detect inaccurate segmentation. For example, segmentation with a non-circular LV blood pool or a blood volume < 50 mL is highly problematic and may indicate poor segmentation.

3.2.2. Comparison between Deep Ensemble, BBB and MC Dropout

In terms of segmentation accuracy and probability calibration, BBB was more robust to noise distortions compared to the other methods. Specifically, BBB showed higher LV Dice, higher LV ASSD, lower NLL, and lower BS on images with greater noise distortions (Figure 2, noise = 0.07, 0.08, 0.10 and Supplementary Tables 1 and 2, degree of distortion = 2, 3, 4). Deep Ensembles was more robust to the blurring and stretching distortions than the other methods. Deep Ensembles showed higher segmentation accuracy in cases with greater blurring and stretching distortions compared to the other methods (Figure 2 and Supplementary Table 1, degree of distortion = 3, 4).

In terms of predictive uncertainty measures, BBB was more robust to the noise distortion while both Deep Ensembles and BBB were more resistant to the blurring compared to the other methods. For example, the mutual information, $Dice_{\text{WithinSamples}}$, and $ASSD_{\text{WithinSamples}}$ uncertainty measures peaked at a noise distortion with degree=3 for BBB. In contrast, the uncertainty measures peaked at a noise distortion with degree=2 for Deep Ensemble, MCD-0.1, and MCD-0.5. Comparing the uncertainty on images with heavy noise distortions (degree of distortion = 3, 4), BBB showed the highest predictive uncertainty. This was followed by MCD-0.5 while Deep Ensembles and MCD-0.1 showed the lowest predictive uncertainties. For images that were heavily blurred, Deep Ensembles and BBB showed the highest

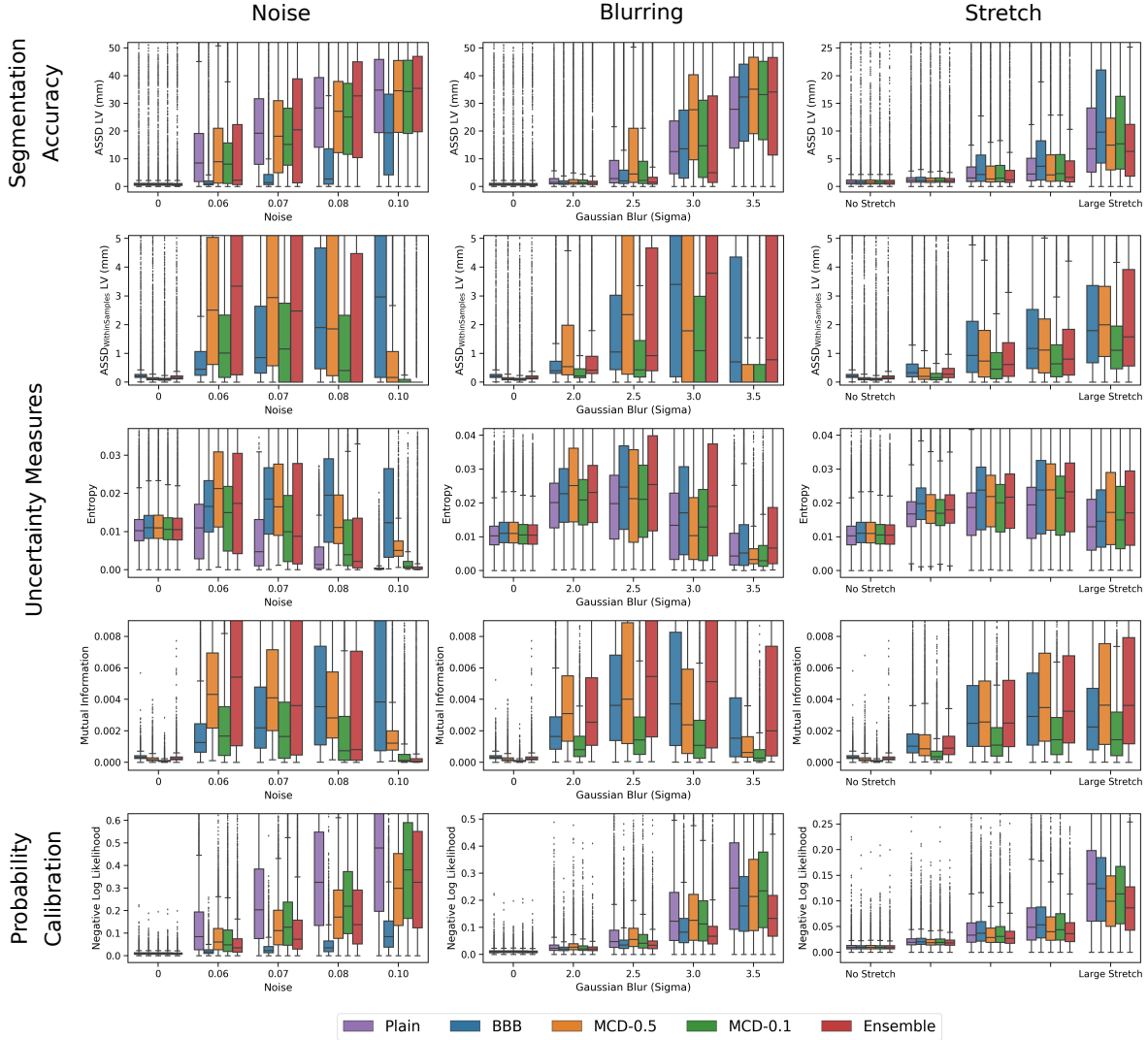


Figure 2: Segmentation accuracy (ASDD LV), uncertainty measures (ASDD_{WithinSamples} LV, entropy, mutual information), and probability calibration (negative log likelihood) on images with increasing amount of noise, blurring, and stretching using a plain U-net, U-net with BBB, MC Dropout, or Deep Ensemble.

predictive uncertainty. In cases of images with stretching distortions, all methods showed fairly similar predictive uncertainty across all degrees of stretching. Having high predictive uncertainties on heavily distorted images is desirable since they have lower segmentation accuracy. Overall, BBB showed good predictive uncertainties on all of the tested distortions while Deep Ensemble showed good predictive uncertainties only in cases of blurring and stretching distortions. MCD-0.1 and MCD-0.5 showed results comparable to BBB and Deep Ensembles only on the stretched datasets.

3.3. Uncertainty on Dataset Shift

To further validate the uncertainty measures, we applied the models trained on the UKBB dataset to a different dataset - the ACDC dataset. The ACDC dataset consists of images with pathologies and image contrast distinctly different from the

UKBB training dataset. Because of the dataset shift, we expect decreased segmentation accuracy and increased predictive uncertainty on the ACDC dataset compared to the UKBB test dataset.

Figure 4 shows the segmentation accuracy and uncertainty metrics of the U-net models tested on the ACDC dataset. As expected, we observed decreased segmentation accuracy and increased predictive uncertainty compared to the UKBB test dataset. In terms of segmentation accuracy and probability calibration, the methods from the best to the worst are: Deep Ensemble, BBB, MCD-0.1, Plain U-net, and MCD-0.5, as shown in Figure 4 and Supplementary Table 4. The methods with the highest to the lowest uncertainties are: MCD-0.5, Deep Ensemble, BBB, and MCD-0.1, as shown in Figure 4 and Supplementary Table 5. Having high uncertainty on a shifted dataset is desirable, especially when the segmentation performance is poor. Over-

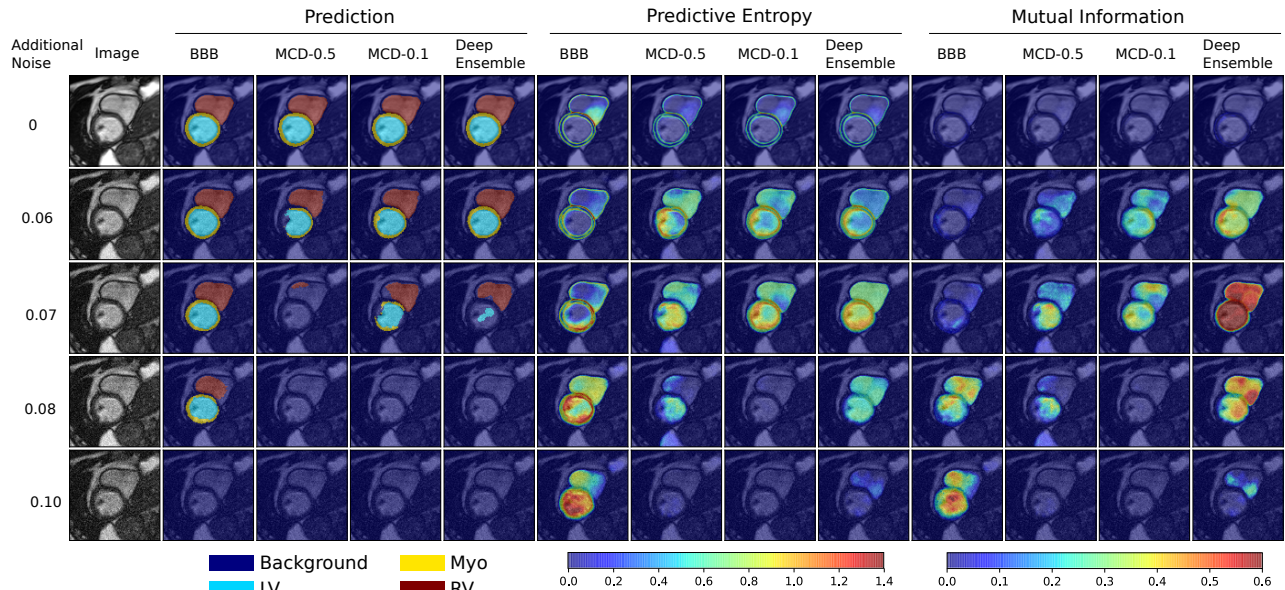


Figure 3: Segmentation predictions and pixelwise uncertainty (predictive entropy, mutual information) on images with increasing noise. Segmentation accuracy decreased while predictive uncertainty increased with more noise. Reproduced by kind permission of UK Biobank ©.

all, both Deep Ensembles and BBB showed good segmentation accuracy and predictive uncertainty in cases of shifted dataset.

3.4. Correlations between Uncertainty and Segmentation Accuracy

To demonstrate the potential utility of uncertainty measures, we evaluated the Spearman rank correlation between uncertainty measures and segmentation accuracy. We used the rank correlation instead of linear correlation to reduce effects of a potential non-linear relationship between the two quantities.

Figure 4 shows the Spearman rank correlation between the uncertainty measures and the ASSD on the UKBB and ACDC test datasets. In the case of training and testing on the UKBB dataset (UKBB \rightarrow UKBB), the uncertainty measure that correlated the most with ASSD was $ASSD_{\text{WithinSamples}}$ (Spearman correlation = [0.58, 0.69]). This is not surprising since $ASSD_{\text{WithinSamples}}$ calculation was similar to ASSD. Similar observations were obtained for training on the UKBB dataset and testing on the ACDC dataset (UKBB \rightarrow ACDC) although the correlations were slightly lower (Spearman correlation = [0.44, 0.66]). These correlations suggest that the $ASSD_{\text{WithinSamples}}$ uncertainty measure is useful in predicting the segmentation quality when ground truth is not available.

Figure 5 shows representative segmentation results, posterior prediction samples, and the structural uncertainty measures for RV. The images with poor segmentation (toward the right side) had greater uncertainty as measured by $Dice_{\text{WithinSamples}}$ and $ASSD_{\text{WithinSamples}}$. Note that posterior prediction samples are not meant to reflect human inter- or intra-observer variability but rather show what the network has learned from the given data.

3.5. Uncertainty for Segmentation Quality Control

In this section, we explored the use of predictive uncertainty estimates to flag potentially problematic segmentations that re-

quire manual review. We view this task as a classification problem and we aim to use uncertainty measures to classify segmentations as either good or poor.

Having experts to manually determine whether an automated segmentation is good or not for a large dataset is time consuming and adds observer noise. Instead, we used thresholds on segmentation accuracies to determine good or poor automated segmentation. Based on our experience and discussions with our clinical collaborators, we think that contour or surface distance is more indicative of inaccurate segmentations. As such, for each method, the predicted segmentation was considered as poor when the ASSD between the prediction and ground truth is greater than the ASSD of inter-observer manual segmentations. We used inter-observer ASSD of 1.17 mm for LV, 1.19 mm for Myo, and 1.88 mm for RV, based on a recent relatively large-scale study (Bai et al., 2018). We then evaluated how well the $ASSD_{\text{WithinSamples}}$ uncertainty measure could identify poor segmentations.

To utilize the $ASSD_{\text{WithinSamples}}$ uncertainty measure, a threshold can be set such that any segmentation with uncertainty above the threshold is flagged for manual review. This would hopefully result in a decreased number of poor segmentation in the dataset. Figure 6 shows the fraction of images with poor segmentation remaining in the dataset and the fraction of images flagged for manual correction when the uncertainty thresholds were varied, i.e., (positives - true positives) vs (true positives + false positives), where positive represents poor segmentation. As we decreased the uncertainty threshold (top left to bottom right in Figure 6), we flagged more images for manual correction and the number of images with poor segmentation was decreased. The first point on the curves corresponds to a threshold where none of the images are reviewed while the last point indicates that all of the images are reviewed.

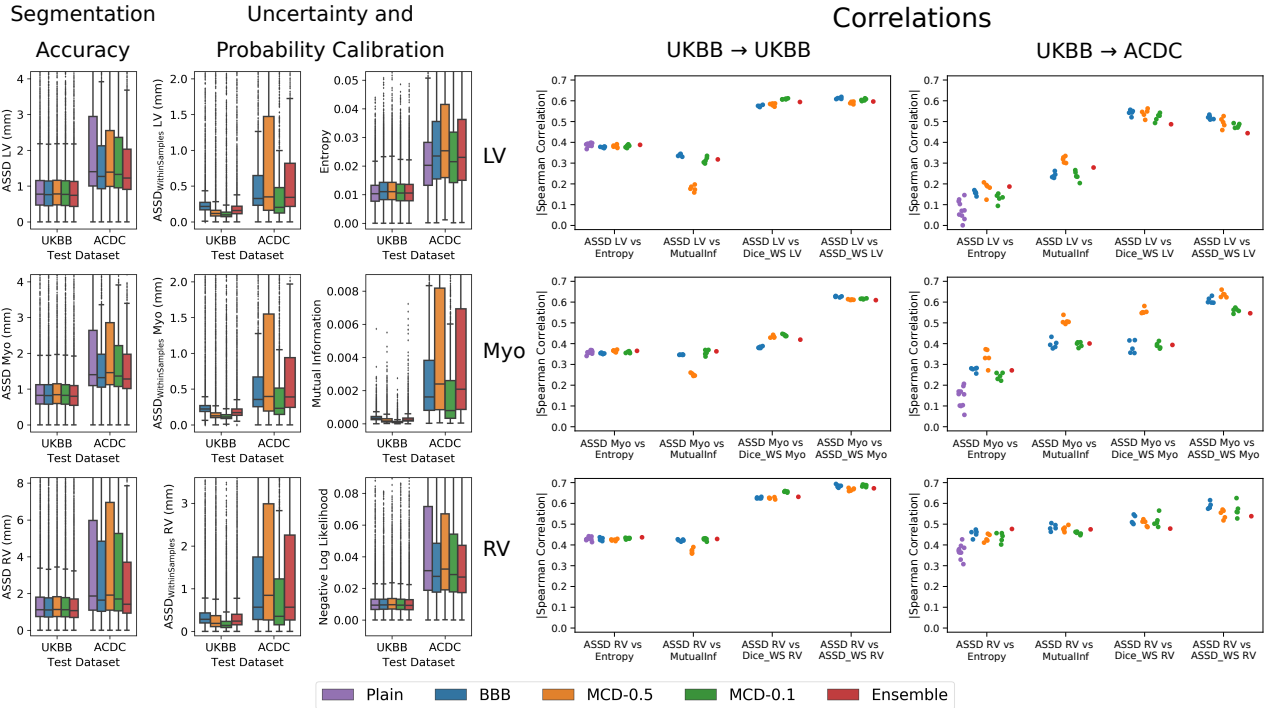


Figure 4: (Left) Segmentation accuracy, predictive uncertainty, and probability calibration of models trained on the UKBB training dataset and tested on the UKBB and ACDC datasets. (Right) Spearman correlations between segmentation accuracy (ASDD) and uncertainty measures (entropy, mutual information, $\text{Dice}_{\text{WithinSamples}}$, $\text{ASDD}_{\text{WithinSamples}}$) on the UKBB and ACDC datasets. Each point represents one run.

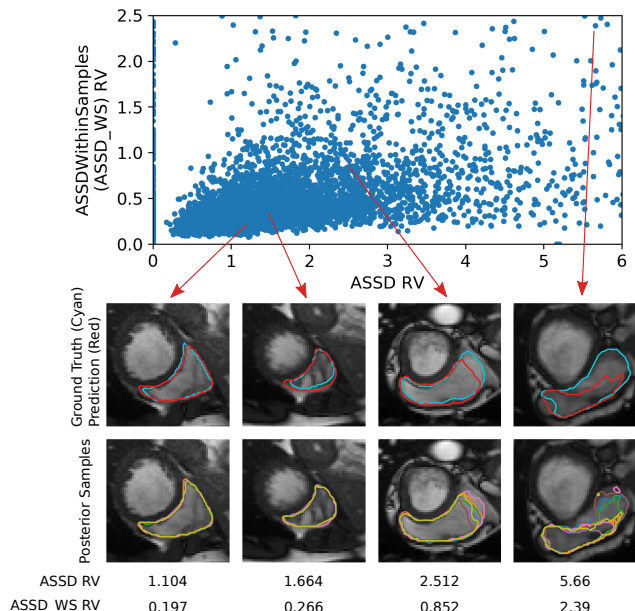


Figure 5: A scatter plot showing the relationship between ASDD and $\text{ASDD}_{\text{WithinSamples}}$ using BBB. Images with manual and predicted segmentations, and posterior segmentation samples illustrate varying ASDD and $\text{ASDD}_{\text{WithinSamples}}$. Reproduced by kind permission of UK Biobank ©.

This is similar to a receiver operating curve with the consideration that the total number of positives or images with poor

predicted segmentation is different for each method. This allows for comparison between all the uncertainty estimation methods. Specifically, a curve closer to the bottom left corner or a curve with smaller area under the curve (AUC) indicates that the algorithm provides better initial segmentation and/or its uncertainty is a good indicator of segmentation accuracy. Figure 6 shows that all the methods performed similarly for detecting poor LV, Myo, and RV segmentation with Deep Ensembles having slightly lower AUC than the other methods.

The thresholds of the uncertainty measures for flagging images for manual review can be adjusted based on the requirements of the application. This approach provides a way to identify images to review and may result in substantial time savings. For example, using the $\text{ASDD}_{\text{WithinSamples}}$ uncertainty measure for the Deep Ensembles method, 48%, 38%, and 31% of the images required manual review in order to reduce the number of images with poor LV, Myo, or RV segmentation to 5% of the test dataset, respectively (Figure 6). In contrast, without using uncertainty measures and assuming no other information about the images is used, approximately 75% of the images need to be reviewed to reduce the proportion of poor segmentation to 5%. Furthermore, using the $\text{ASDD}_{\text{WithinSamples}}$ uncertainty measure resulted in more time savings compared to a naive approach of reviewing images based on slice position. Specifically, since the segmentation is usually worse on basal and apical slices, a naive approach for segmentation quality control is to first review all of the most basal and most apical slices, followed by the second-most basal and second-most apical slices, and so on. We

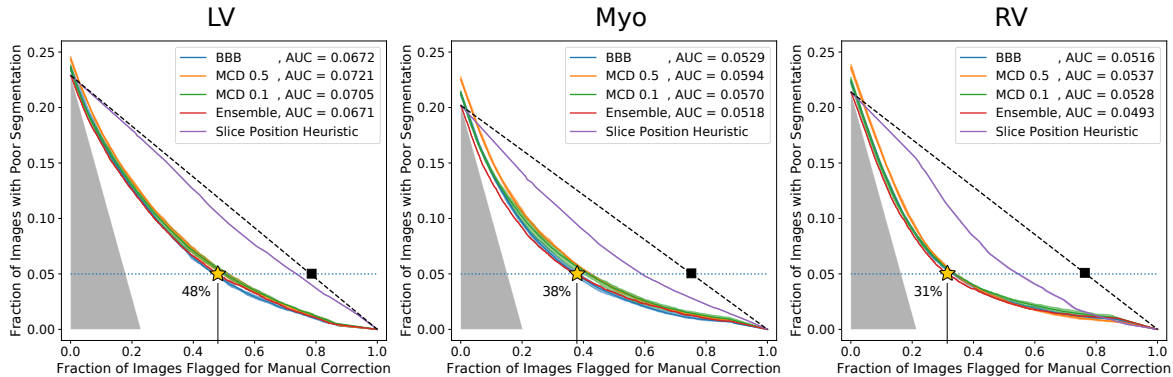


Figure 6: Fraction of images with poor segmentation remaining (based on a threshold on ASSD between predicted and ground truth segmentation) after flagging images for manual correction using $ASSD_{WithinSamples}$ from BBB, MC Dropout, or Deep Ensembles. Dotted black line shows flagging images for manual segmentation randomly. Shaded area shows the ideal region where all images flagged for manual correction directly reduce the number of poor segmentations.

refer to this approach as using the slice position as a heuristic for segmentation quality control. As shown in Figure 6, using uncertainty measures is more advantageous than this naive approach as evidenced by a lower AUC and a smaller number of images to review to have 5% poor segmentation remaining. Assuming a dataset of 10,000 subjects each with 10 slices and manual segmentation of 30 seconds per structure per slice (Bai et al., 2018), using the $ASSD_{WithinSamples}$ uncertainty measure results in ~ 940 hours of time savings compared to reviewing the images randomly, and ~ 580 hours of time savings compared to using the slice position heuristic to achieve 5% poor segmentation remaining.

3.6. Training Time

All experiments were performed on an Nvidia P100 GPU with 12GB of memory. MC Dropout and BBB required ~ 35 hours and ~ 47 hours for training, respectively. For these Bayesian methods, generating 50 prediction samples during testing required 1.5 seconds for each 2D image. The Deep Ensembles method consisted of 10 copies of the plain U-net and was trained in parallel separately. Each plain U-net required ~ 12 hours for training and ~ 0.1 seconds for prediction of a 2D image. Calculation of the predictive entropy, mutual information, $Dice_{WithinSamples}$, and $ASSD_{WithinSamples}$ uncertainty measures required approximately 0.05, 0.15, 0.15, and 0.4 seconds per image, respectively.

4. Discussion

4.1. BBB vs MC Dropout vs Deep Ensemble

In this work, we evaluated and compared different Bayesian and non-Bayesian approaches for estimating uncertainty in neural networks for cardiac MRI segmentation. Here, we discuss similarities and differences about how uncertainty is learned in these methods, what was learned after training, and relate these differences to the quality of the predictive uncertainties on out-of-distribution images.

While uncertainty in neural network parameters is learned automatically in BBB, this can be tuned by changing the dropout

rate in MC Dropout. For the UKBB dataset, a small dropout rate of 0.1 in the middle layers performed better than other MC Dropout models in terms of segmentation accuracy and probability calibration. This is different from other studies which commonly used a dropout rate of 0.5 (Wang et al., 2019a; Kendall et al., 2017) and may be because of the large amount of relatively uniform training data (i.e., images acquired following the same MR protocol and labelled following the same guidelines). The dropout rate hyperparameters for MC Dropout obtained through grid search correspond to the weight uncertainties learned by BBB to some extent. Figure 7 shows that the standard deviation of the weights learned by BBB is lower in the early layers and higher in the middle layers of the U-net. This is similar to MC Dropout with no dropout in the early layers and some dropout on the middle layers. Having greater dropout rate in middle layers is common in other studies (Kendall et al., 2017).

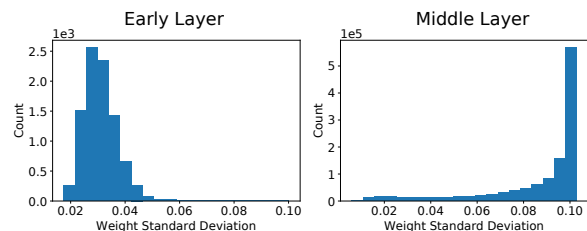


Figure 7: Histogram of learned weight standard deviations in the early and middle layers from BBB.

The effect of dropout rate in MC Dropout is shown in the experiments with dataset shift (Figure 4, left). A dropout rate of 0.1 yielded higher segmentation accuracy but lower uncertainty whereas a dropout rate of 0.5 resulted in lower segmentation accuracy but higher predictive uncertainty. BBB was able to mitigate this issue by learning a mean and standard deviation for each weight, resulting in comparable or higher segmentation accuracy with moderate predictive uncertainties between MCD-0.1 and MCD-0.5 (Figure 4, left).

In Deep Ensembles, the uncertainty in the weights is not learned or tuned but instead stems from the random initialization

of the weights and stochasticity of the training procedure. Each model in the ensemble would then learn a local minimum which are combined to form a prediction and uncertainty estimate. This was found to outperform BBB in terms of segmentation accuracy and probability calibration in most cases. This may be because the approximate posterior learned by BBB covered only one (or a few) mode(s) of the true posterior and a small neighbourhood around each mode, as opposed to multiple local modes in Deep Ensembles. Based on our observations, the histogram of the weights learned by each member in Deep Ensembles was very similar to each other. Techniques such as canonical correlation analysis can be used to compare the representations (i.e., feature maps) between different members of the ensemble and to better understand model uncertainty (Morcos et al., 2018).

While Deep Ensembles performed similarly or better than BBB on images with blurring or stretching distortions, BBB outperformed Deep Ensembles on images with noise distortions. A difference in these distortions is that the noise was added independently per pixel while blurring and stretching were applied for each structure as a whole. This suggests that BBB is more suitable for capturing uncertainty in low-level pixelwise variations while Deep Ensemble is better for modelling uncertainty in structural variations.

Bayesian approaches and Deep Ensembles can be used to improve segmentation accuracy on datasets which are slightly shifted compared to the training dataset. While the segmentation accuracies for testing on the ACDC dataset using the models trained on UKBB dataset are lower than segmentation accuracies obtained using models trained and tested both on the ACDC dataset (Bernard et al., 2018), the algorithms employed in this work may be combined with other techniques that are specifically designed to solve this problem, e.g., style augmentation or domain adversarial training (Ly et al., 2019; Ganin et al., 2016).

4.2. Pixelwise and Structural Uncertainty Measures

We introduced pixelwise and structural uncertainty measures to quantify the predictive uncertainty, and demonstrated the utility of these metrics for segmentation quality control. Both pixelwise and structural uncertainty measures can be used depending on the application. As the segmentation problem was formulated as pixel classification, pixelwise uncertainty measures are straightforward to obtain. These allow users to visualize which pixels and which areas are potentially problematic (Figure 3). However, segmentation is often performed at the image-level and slice by slice. Therefore, in developing uncertainty measures for determining problematic segmentation, an image-level uncertainty measure is required. Accordingly, we showed that structural uncertainty measures are correlated with segmentation accuracy metrics such as ASSD.

It is important to note that the predictive uncertainty measures reflect the neural network uncertainty, which is different from human uncertainty. An example is the image with heavy noise in the last row in Figure 3. It is expected that human observers can manually segment this image with low observer variability; however, since the image is very different from the training data, the neural networks were not able to generate a reasonable

segmentation and showed high predictive entropy and mutual information for the entire cardiac structure.

4.3. Segmentation Quality Control

We showed that the uncertainty measures have decent to good correlations with segmentation accuracy. This could have been negatively affected by noisy ground truth segmentation. Framing segmentation quality control as a binary classification problem instead of evaluating the correlations or predicting the segmentation accuracy metrics alleviates the problem of noise in ground truth segmentation. In this regard, we defined poor segmentation using a threshold on the ASSD between the predicted and ground truth segmentation. This definition of a poor segmentation was adopted based on discussions with clinical collaborators; however, it can be modified depending on the application. For example, other segmentation accuracy metrics such as Hausdorff distance or misclassification area can be used and the framework for evaluating uncertainty measures described in this work can be applied directly.

Other studies in segmentation quality control include directly predicting segmentation accuracy or comparing the predicted segmentation to a reference database. Albà et al. (2018) trained a random forest classifier to predict a binary label of correct or incorrect segmentation. The examples of correct segmentation were generated using the ground truth segmentations while the incorrect segmentations were generated by deforming or translating the ground truth segmentations. Robinson et al. (2018) used a 3D residual network to directly predict the Dice score of a segmentation from an image-segmentation pair. The network was trained and tested on a dataset created using a random forest segmentation algorithm. These classifiers are agnostic to how the segmentation was generated. However, these approaches are dependent on training with some expected segmentation failures, which may be challenging to incorporate during training. In contrast, our approach used uncertainty measures to detect poor segmentation and is explainable. Instead of using a learning algorithm to determine segmentation quality, we used model uncertainty which emerges intrinsically when training the segmentation algorithm. A slight limitation of our approach is that sampling during the testing phase required up to 50x more computation time compared to a single prediction but this may be accelerated through parallelization.

Another approach for segmentation quality control is using a modified version of Reverse Classification Accuracy to predict the segmentation quality of an image-segmentation pair (Robinson et al., 2019). This approach requires a reference database of images with ground truth segmentation. Each reference image is registered to the test image and the associated reference segmentations are warped accordingly. The warped reference segmentations are considered as potential segmentations of the test image. The quality of the test image segmentation is estimated by comparing the potential segmentations and test segmentation. A limitation of this approach is that it requires a long time to generate the segmentation quality prediction, mainly due to the registration steps.

5. Conclusions

In this work, we compared Bayesian and non-Bayesian methods, namely BBB, MC Dropout, and Deep Ensembles for cardiac MRI segmentation and showed the utility of these algorithms for segmentation quality control. We found that Deep Ensembles performed better in terms of segmentation accuracy and probability calibration on in-distribution and out-of-distribution datasets. However, BBB outperformed Deep Ensembles on images with noise distortions. Additionally, we identified a limitation of current methods in terms of predictive uncertainty on images with heavy distortions. Furthermore, we showed that the $ASSD_{\text{WithinSamples}}$ uncertainty measure correlated well with the ASSD segmentation accuracy on both in-distribution and out-of-distribution datasets. For the task of segmentation quality control, $ASSD_{\text{WithinSamples}}$ from all methods are equally useful in predicting problematic segmentations. Using uncertainty measures can result in substantial time savings by reducing the number of images that needs to be reviewed.

Acknowledgments

We acknowledge the use of the facilities of Compute Canada. This work was funded by Canadian Institutes of Health Research (CIHR) MOP: #93531, Ontario Research Fund and GE Healthcare. FG is supported by a Banting postdoctoral fellowship.

This work was partly funded by the European Union's Horizon 2020 research and innovation programme under grant agreement No 825903 (euCanSHare project). SEP acts as a paid consultant to Circle Cardiovascular Imaging Inc., Calgary, Canada and Servier. SEP acknowledges support from the National Institute for Health Research (NIHR) Biomedical Research Centre at Barts, from the SmartHeart EPSRC programme grant (EP/P001009/1) and the London Medical Imaging and AI Centre for Value-Based Healthcare. SEP acknowledges support from the CAP-AI programme, London's first AI enabling programme focused on stimulating growth in the capital's AI sector. SEP, SN and SKP acknowledge the British Heart Foundation for funding the manual analysis to create a cardiovascular magnetic resonance imaging reference standard for the UK Biobank imaging resource in 5000 CMR scans (PG/14/89/31194). This project was enabled through access to the Medical Research Council eMedLab Medical Bioinformatics infrastructure, supported by the Medical Research Council (MR/L016311/1).

Availability of the data

This research was conducted using the UK Biobank resource under Application 2964. UK Biobank will make the data available to all bona fide researchers for all types of health-related research that is in the public interest, without preferential or exclusive access for any person. All researchers will be subject to the same application process and approval criteria as specified by UK Biobank. For the detailed access procedure see <http://www.ukbiobank.ac.uk/register-apply/>.

References

- Albà, X., Lekadir, K., Pereañez, M., Medrano-Gracia, P., Young, A.A., Frangi, A.F., 2018. Automatic initialization and quality control of large-scale cardiac mri segmentations. *Medical image analysis* 43, 129–141.
- Bai, W., Sinclair, M., Tarroni, G., Oktay, O., Rajchl, M., Vaillant, G., Lee, A.M., Aung, N., Lukaschuk, E., Sanghvi, M.M., et al., 2018. Automated cardiovascular magnetic resonance image analysis with fully convolutional networks. *Journal of Cardiovascular Magnetic Resonance* 20, 65.
- Bernard, O., Lalonde, A., Zotti, C., Cervenansky, F., Yang, X., Heng, P.A., Cetin, I., Lekadir, K., Camara, O., Ballester, M.A.G., et al., 2018. Deep learning techniques for automatic mri cardiac multi-structures segmentation and diagnosis: Is the problem solved? *IEEE Transactions on Medical Imaging*.
- Bishop, C.M., 1994. Novelty detection and neural network validation. *IEE Proceedings-Vision, Image and Signal processing* 141, 217–222.
- Blundell, C., Cornebise, J., Kavukcuoglu, K., Wierstra, D., 2015. Weight uncertainty in neural network, in: *International Conference on Machine Learning*, pp. 1613–1622.
- DeVries, T., Taylor, G.W., 2018. Leveraging uncertainty estimates for predicting segmentation quality. *arXiv preprint arXiv:1807.00502*.
- Efron, B., Tibshirani, R., 1986. Bootstrap methods for standard errors, confidence intervals, and other measures of statistical accuracy. *Statistical science*, 54–75.
- Fortunato, M., Blundell, C., Vinyals, O., 2017. Bayesian recurrent neural networks. *arXiv preprint arXiv:1704.02798*.
- Gal, Y., 2016. Uncertainty in deep learning. Ph.D. thesis. University of Cambridge.
- Gal, Y., Ghahramani, Z., 2016. Dropout as a bayesian approximation: Representing model uncertainty in deep learning, in: *international conference on machine learning*, pp. 1050–1059.
- Ganin, Y., Ustinova, E., Ajakan, H., Germain, P., Larochelle, H., Laviolette, F., Marchand, M., Lempitsky, V., 2016. Domain-adversarial training of neural networks. *The Journal of Machine Learning Research* 17, 2096–2030.
- Gudbjartsson, H., Patz, S., 1995. The rician distribution of noisy mri data. *Magnetic resonance in medicine* 34, 910–914.
- Guo, C., Pleiss, G., Sun, Y., Weinberger, K.Q., 2017. On calibration of modern neural networks, in: *Proceedings of the 34th International Conference on Machine Learning-Volume 70, JMLR. org*. pp. 1321–1330.
- Hann, E., Biasioli, L., Zhang, Q., Popescu, I.A., Werys, K., Lukaschuk, E., Carapella, V., Paiva, J.M., Aung, N., Rayner, J.J., et al., 2019. Quality control-driven image segmentation towards reliable automatic image analysis in large-scale cardiovascular magnetic resonance aortic cine imaging, in: *International Conference on Medical Image Computing and Computer-Assisted Intervention, Springer*. pp. 750–758.
- Hoffman, M.D., Blei, D.M., Wang, C., Paisley, J., 2013. Stochastic variational inference. *The Journal of Machine Learning Research* 14, 1303–1347.
- Jungo, A., Balsiger, F., Reyes, M., 2020. Analyzing the quality and challenges of uncertainty estimations for brain tumor segmentation. *Frontiers in Neuroscience* 14, 282.
- Jungo, A., Meier, R., Ermis, E., Herrmann, E., Reyes, M., 2018. Uncertainty-driven sanity check: Application to postoperative brain tumor cavity segmentation, in: *Medical Imaging with Deep Learning*.
- Jungo, A., Reyes, M., 2019. Assessing reliability and challenges of uncertainty estimations for medical image segmentation, in: *International Conference on Medical Image Computing and Computer-Assisted Intervention, Springer*. pp. 48–56.
- Kendall, A., Badrinarayanan, V., Cipolla, R., 2017. Bayesian segnet: Model uncertainty in deep convolutional encoder-decoder architectures for scene understanding, in: *British Machine Vision Conference 2017, BMVC 2017*.
- Kingma, D.P., Salimans, T., Welling, M., 2015. Variational dropout and the local reparameterization trick, in: *Advances in Neural Information Processing Systems*, pp. 2575–2583.
- Lakshminarayanan, B., Pritzel, A., Blundell, C., 2017. Simple and scalable predictive uncertainty estimation using deep ensembles, in: *Advances in Neural Information Processing Systems*, pp. 6402–6413.
- Louizos, C., Welling, M., 2017. Multiplicative normalizing flows for variational bayesian neural networks, in: *Proceedings of the 34th International Conference on Machine Learning-Volume 70, JMLR. org*. pp. 2218–2227.
- Ly, B., Cochet, H., Serresant, M., 2019. Style data augmentation for robust segmentation of multi-modality cardiac mri, in: *Statistical Atlases and Computational Modelling of the Heart*.

- MacKay, D.J., 1995. Probable networks and plausible predictions—a review of practical bayesian methods for supervised neural networks. *Network: computation in neural systems* 6, 469–505.
- Mehrtash, A., Wells, W.M., Tempny, C.M., Abolmaesumi, P., Kapur, T., 2020. Confidence calibration and predictive uncertainty estimation for deep medical image segmentation. *IEEE Transactions on Medical Imaging* .
- Morcos, A., Raghu, M., Bengio, S., 2018. Insights on representational similarity in neural networks with canonical correlation, in: *Advances in Neural Information Processing Systems*, pp. 5727–5736.
- Nair, T., Precup, D., Arnold, D.L., Arbel, T., 2019. Exploring uncertainty measures in deep networks for multiple sclerosis lesion detection and segmentation. *Medical Image Analysis* , 101557.
- Neal, R.M., 2012. Bayesian learning for neural networks. volume 118. Springer Science & Business Media.
- Osband, I., 2016. Risk versus uncertainty in deep learning: Bayes, bootstrap and the dangers of dropout, in: *Proceedings of the NIPS* 2016 Workshop on Bayesian Deep Learning*.
- Peng, P., Lekadir, K., Gooya, A., Shao, L., Petersen, S.E., Frangi, A.F., 2016. A review of heart chamber segmentation for structural and functional analysis using cardiac magnetic resonance imaging. *Magnetic Resonance Materials in Physics, Biology and Medicine* 29, 155–195.
- Petersen, S.E., Matthews, P.M., Francis, J.M., Robson, M.D., Zemrak, F., Boubertakh, R., Young, A.A., Hudson, S., Weale, P., Garratt, S., et al., 2015. Uk biobank’s cardiovascular magnetic resonance protocol. *Journal of cardiovascular magnetic resonance* 18, 8.
- Robinson, R., Oktay, O., Bai, W., Valindria, V.V., Sanghvi, M.M., Aung, N., Paiva, J.M., Zemrak, F., Fung, K., Lukaszuk, E., Lee, A.M., Carapella, V., Kim, Y.J., Kainz, B., Piechnik, S.K., Neubauer, S., Petersen, S.E., Page, C., Rueckert, D., Glocker, B., 2018. Real-time prediction of segmentation quality, in: Frangi, A.F., Schnabel, J.A., Davatzikos, C., Alberola-López, C., Fichtinger, G. (Eds.), *International Conference on Medical Image Computing and Computer-Assisted Intervention*. Springer. pp. 578–585.
- Robinson, R., Valindria, V.V., Bai, W., Oktay, O., Kainz, B., Suzuki, H., Sanghvi, M.M., Aung, N., Paiva, J.M., Zemrak, F., et al., 2019. Automated quality control in image segmentation: application to the uk biobank cardiovascular magnetic resonance imaging study. *Journal of Cardiovascular Magnetic Resonance* 21, 18.
- Ronneberger, O., Fischer, P., Brox, T., 2015. U-net: Convolutional networks for biomedical image segmentation, in: Navab, N., Hornegger, J., Wells, W.M., Frangi, A.F. (Eds.), *International Conference on Medical image computing and computer-assisted intervention*, Springer. pp. 234–241.
- Roy, A.G., Conjeti, S., Navab, N., Wachinger, C., 2018. Inherent brain segmentation quality control from fully convnet monte carlo sampling, in: Frangi, A.F., Schnabel, J.A., Davatzikos, C., Alberola-López, C., Fichtinger, G. (Eds.), *International Conference on Medical Image Computing and Computer-Assisted Intervention*, Springer. pp. 664–672.
- Ruijsink, B., Puyol-Antón, E., Oksuz, I., Sinclair, M., Bai, W., Schnabel, J.A., Razavi, R., King, A.P., 2019. Fully automated, quality-controlled cardiac analysis from cmr: validation and large-scale application to characterize cardiac function. *JACC: Cardiovascular Imaging* .
- Sander, J., de Vos, B.D., Wolterink, J.M., Išgum, I., 2019. Towards increased trustworthiness of deep learning segmentation methods on cardiac mri, in: *Medical Imaging 2019: Image Processing*, International Society for Optics and Photonics. p. 1094919.
- Schulam, P., Saria, S., 2019. Can you trust this prediction? auditing pointwise reliability after learning, in: *The 22nd International Conference on Artificial Intelligence and Statistics*, pp. 1022–1031.
- Wang, G., Li, W., Aertsen, M., Deprest, J., Ourselin, S., Vercauteren, T., 2019a. Aleatoric uncertainty estimation with test-time augmentation for medical image segmentation with convolutional neural networks. *Neurocomputing* 338, 34–45.
- Wang, G., Li, W., Vercauteren, T., Ourselin, S., 2019b. Automatic brain tumor segmentation based on cascaded convolutional neural networks with uncertainty estimation. *Frontiers in computational neuroscience* 13, 56.
- Wen, Y., Vicol, P., Ba, J., Tran, D., Grosse, R., 2018. Flipout: Efficient pseudo-independent weight perturbations on mini-batches. *International Conference on Learning Representations (ICLR)* .

Supplementary Material

Please see the supplementary material for detailed tables of results.

Supplementary Material to “Estimating Uncertainty in Neural Networks for Cardiac MRI Segmentation: A Benchmark Study”

Matthew Ng^{a,b,*}, Fumin Guo^{a,b}, Labonny Biswas^a, Steffen E. Petersen^{c,d}, Stefan K. Piechnik^e, Stefan Neubauer^e, Graham Wright^{a,b}

^aPhysical Sciences Platform, Sunnybrook Research Institute, Toronto, ON, Canada

^bDepartment of Medical Biophysics, University of Toronto, Toronto, ON, Canada

^cWilliam Harvey Research Institute, NIHR Barts Biomedical Research Centre, Queen Mary University of London, UK

^dBarts Heart Centre, St Bartholomew's Hospital, Barts Health NHS Trust, West Smithfield, London, UK

^eDivision of Cardiovascular Medicine, Oxford NIHR Biomedical Research Centre, Radcliffe Department of Medicine, University of Oxford, Oxford, UK

arXiv:2012.15772v1 [eess.IV] 31 Dec 2020

*Corresponding author: 2075 Bayview Avenue, Toronto, ON M4N 3M5.
Email: matthewng@mail.utoronto.ca (Matthew Ng)

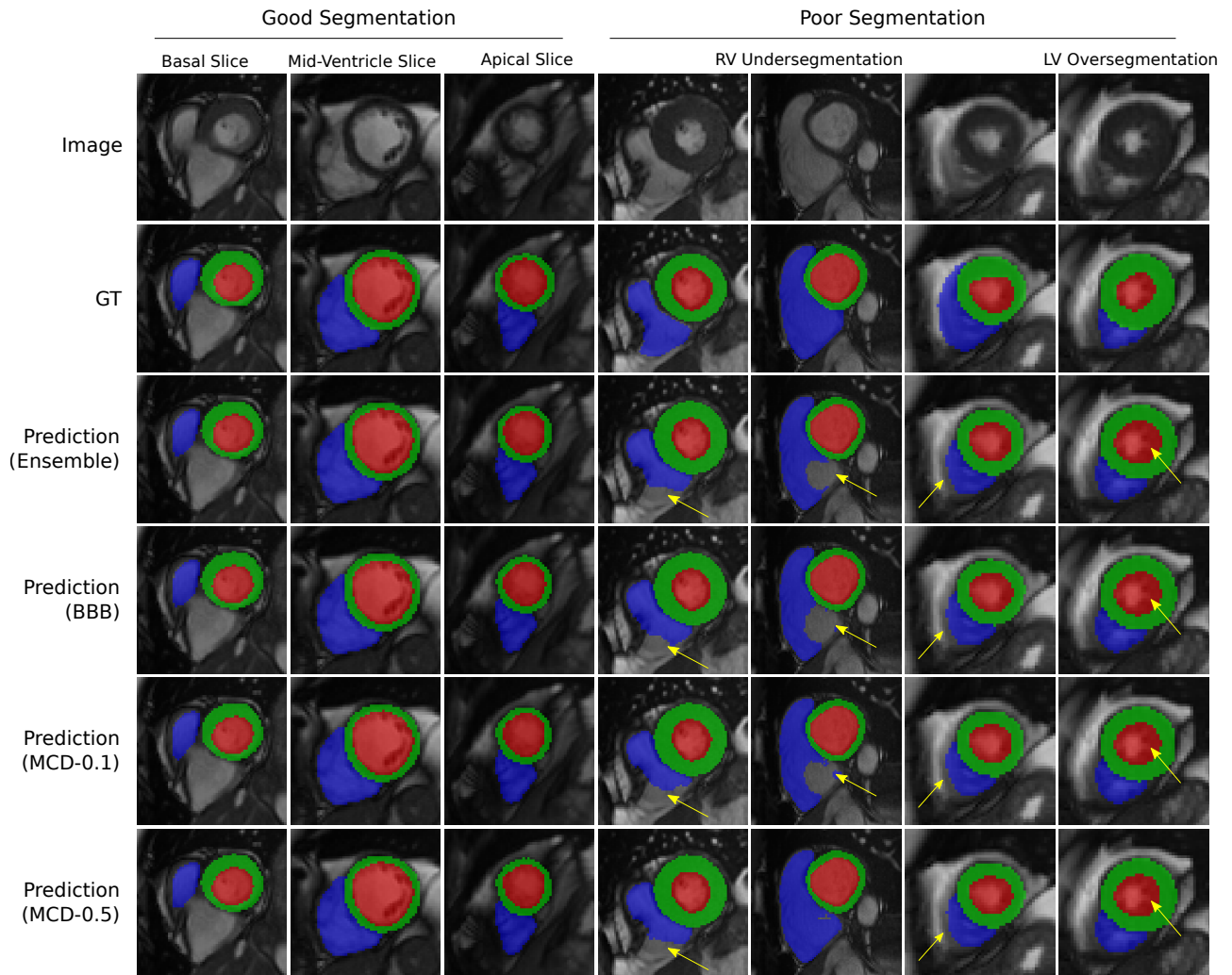


Figure 1: Example segmentation results using the U-net with Deep Ensembles, BBB, and MC Dropout (MCD). Red = LV, green = Myo, blue = RV. Yellow arrows show area of inaccurate segmentation. Note that all methods have similar results. Reproduced by kind permission of UK Biobank ©.

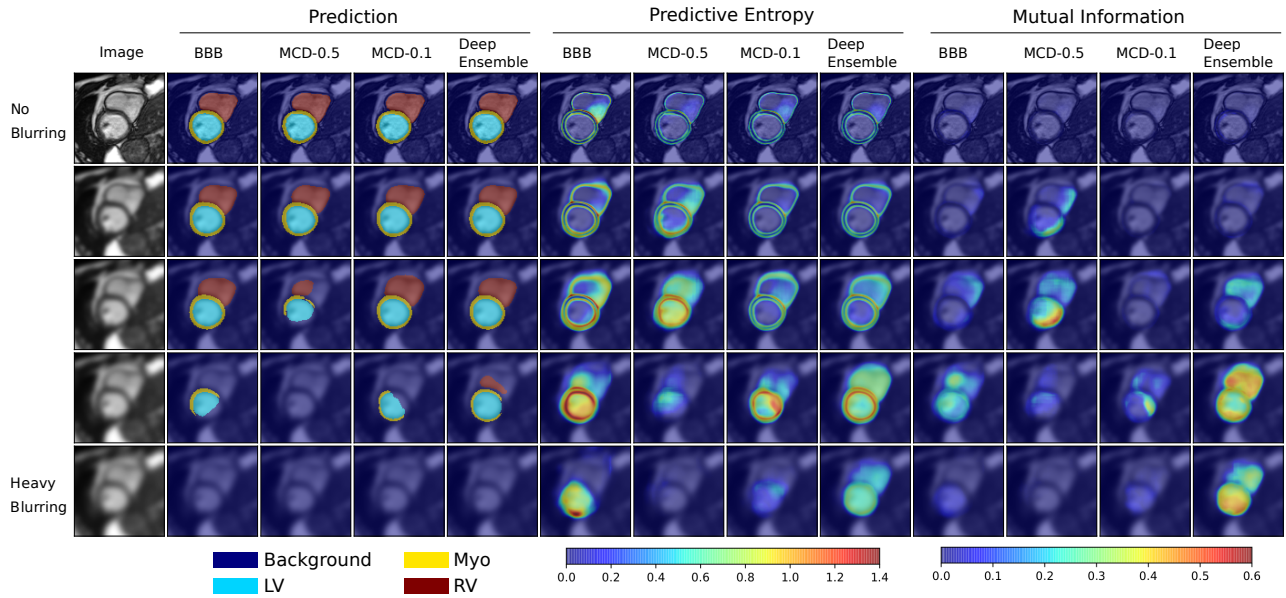


Figure 2: Segmentation predictions and pixelwise uncertainty on images with increasing blur. Segmentation accuracy decreases while predictive uncertainty increases with more blurring. Reproduced by kind permission of UK Biobank ©.

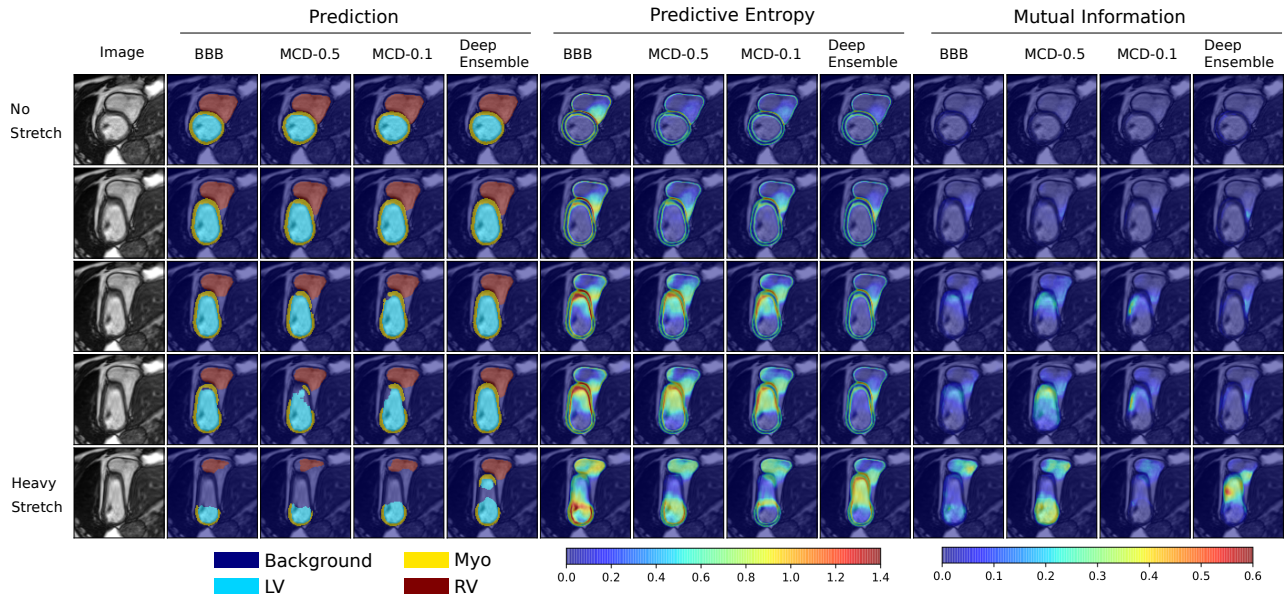


Figure 3: Segmentation predictions and pixelwise uncertainty on images with increasing stretch. Segmentation accuracy decreases while predictive uncertainty increases with more stretch. Reproduced by kind permission of UK Biobank ©.

Table 1: Segmentation accuracy metrics on images with increasing noise, blurring, or stretching distortions. Format: Median_{25th percentile-75th percentile}

		Degree of Distortion					
		0	1	2	3	4	
Noise	Pixelwise Accuracy	Plain	.9960 _{.9944-.9973}	.9841 _{.9716-.9926}	.9749 _{.9599-.9887}	.9686 _{.9525-.9862}	.9648 _{.9464-.9854}
		BBB	.9960 _{.9944-.9973}	.9929_{.9888-.9956}	.9905_{.9833-.9947}	.9862_{.9754-.9932}	.9735_{.9593-.9883}
		MCD-0.5	.9959 _{.9942-.9972}	.9807 _{.9673-.9913}	.9729 _{.9582-.9879}	.9678 _{.9514-.9859}	.9647 _{.9461-.9854}
		MCD-0.1	.9960 _{.9944-.9973}	.9852 _{.9743-.9932}	.9767 _{.9627-.9889}	.9700 _{.9542-.9864}	.9649 _{.9467-.9854}
		Ensemble	.9961_{.9945-.9973}	.9873 _{.9717-.9941}	.9754 _{.9568-.9910}	.9679 _{.9495-.9871}	.9645 _{.9456-.9854}
	Dice LV	Plain	.963 _{.932-.981}	.653 _{.194-.900}	.224 _{.010-.714}	.031 _{.000-.357}	.000 _{.000-.001}
		BBB	.964 _{.934-.982}	.947_{.863-.976}	.927_{.701-.972}	.828_{.307-.961}	.162_{.000-.753}
		MCD-0.5	.963 _{.933-.981}	.657 _{.081-.944}	.235 _{.000-.762}	.000 _{.000-.452}	.000 _{.000-.000}
		MCD-0.1	.963 _{.934-.982}	.714 _{.271-.951}	.356 _{.000-.753}	.024 _{.000-.529}	.000 _{.000-.000}
		Ensemble	.965_{.936-.983}	.873 _{.000-.970}	.000 _{.000-.937}	.000 _{.000-.000}	.000 _{.000-.000}
	ASSD LV	Plain	0.77 _{0.47-1.15}	8.51 _{1.79-19.14}	19.24 _{8.03-31.70}	28.37 _{14.20-39.34}	34.85 _{19.52-45.93}
		BBB	0.76 _{0.45-1.14}	1.07_{0.61-2.05}	1.42_{0.69-4.40}	2.71_{0.88-13.65}	19.44_{4.20-33.37}
MCD-0.5		0.78 _{0.47-1.16}	8.99 _{1.23-21.06}	18.19 _{5.02-31.04}	27.22 _{12.21-37.95}	34.63 _{19.59-45.52}	
MCD-0.1		0.77 _{0.46-1.15}	8.11 _{1.10-15.77}	15.23 _{7.73-28.31}	25.11 _{11.62-37.28}	34.32 _{19.19-45.60}	
Ensemble		0.74_{0.43-1.12}	2.30 _{0.73-22.35}	20.49 _{1.36-38.93}	32.75 _{10.46-45.01}	35.45 _{19.79-47.01}	
Gaussian Blur	Pixelwise Accuracy	Plain	.9960 _{.9944-.9973}	.9910 _{.9868-.9942}	.9842 _{.9759-.9913}	.9732_{.9609-.9878}	.9664_{.9494-.9856}
		BBB	.9960 _{.9944-.9973}	.9922 _{.9889-.9948}	.9864 _{.9779-.9921}	.9726 _{.9583-.9876}	.9656 _{.9465-.9855}
		MCD-0.5	.9959 _{.9942-.9972}	.9894 _{.9829-.9936}	.9779 _{.9637-.9904}	.9676 _{.9491-.9869}	.9647 _{.9456-.9854}
		MCD-0.1	.9960 _{.9944-.9973}	.9915 _{.9873-.9945}	.9847 _{.9747-.9917}	.9713 _{.9563-.9875}	.9652 _{.9461-.9854}
		Ensemble	.9961_{.9945-.9973}	.9923_{.9887-.9950}	.9871_{.9780-.9926}	.9730 _{.9580-.9881}	.9655 _{.9460-.9855}
	Dice LV	Plain	.963 _{.932-.981}	.910 _{.818-.959}	.833 _{.616-.931}	.535 _{.127-.780}	.093_{.000-.349}
		BBB	.964 _{.934-.982}	.936 _{.869-.967}	.883 _{.659-.949}	.466 _{.000-.807}	.000 _{.000-.180}
		MCD-0.5	.963 _{.933-.981}	.922 _{.829-.963}	.726 _{.191-.915}	.066 _{.000-.491}	.000 _{.000-.000}
		MCD-0.1	.964 _{.934-.982}	.928 _{.838-.964}	.864 _{.549-.952}	.356 _{.000-.790}	.000 _{.000-.129}
		Ensemble	.965_{.936-.983}	.940_{.876-.970}	.914_{.775-.964}	.688_{.000-.928}	.000 _{.000-.000}
	ASSD LV	Plain	0.77 _{0.47-1.15}	1.50 _{0.96-2.86}	2.91 _{1.37-9.46}	12.59 _{4.59-23.71}	27.88_{13.87-39.61}
		BBB	0.76 _{0.45-1.14}	1.26 _{0.80-2.01}	2.06 _{1.13-5.93}	13.61 _{3.03-27.63}	32.37 _{16.40-44.20}
MCD-0.5		0.78 _{0.47-1.16}	1.43 _{0.88-2.48}	4.49 _{1.48-21.05}	27.73 _{9.68-40.34}	35.11 _{19.08-46.65}	
MCD-0.1		0.76 _{0.46-1.15}	1.35 _{0.86-2.31}	2.22 _{1.12-9.11}	14.70 _{3.25-31.19}	33.21 _{16.91-45.17}	
Ensemble		0.74_{0.43-1.12}	1.22_{0.74-1.94}	1.58_{0.89-3.34}	4.99_{1.47-32.70}	34.17 _{11.37-46.57}	
Stretch	Pixelwise Accuracy	Plain	.9960 _{.9944-.9973}	.9921 _{.9896-.9940}	.9879 _{.9820-.9925}	.9841 _{.9767-.9912}	.9729 _{.9645-.9852}
		BBB	.9960 _{.9944-.9973}	.9918 _{.9889-.9939}	.9849 _{.9767-.9916}	.9793 _{.9698-.9895}	.9684 _{.9577-.9834}
		MCD-0.5	.9959 _{.9942-.9972}	.9924 _{.9897-.9942}	.9887 _{.9816-.9928}	.9846 _{.9757-.9913}	.9720 _{.9628-.9846}
		MCD-0.1	.9960 _{.9944-.9973}	.9922 _{.9897-.9941}	.9881 _{.9817-.9926}	.9837 _{.9761-.9911}	.9722 _{.9638-.9845}
		Ensemble	.9961_{.9945-.9973}	.9925_{.9902-.9944}	.9894_{.9826-.9933}	.9857_{.9768-.9923}	.9730_{.9638-.9864}
	Dice LV	Plain	.963 _{.932-.981}	.945 _{.895-.969}	.902 _{.762-.963}	.861 _{.697-.955}	.648 _{.402-.838}
		BBB	.964 _{.934-.982}	.946 _{.886-.970}	.856 _{.644-.960}	.778 _{.541-.944}	.530 _{.210-.754}
		MCD-0.5	.963 _{.933-.981}	.949 _{.900-.971}	.916 _{.739-.967}	.862 _{.654-.961}	.626 _{.358-.809}
		MCD-0.1	.964 _{.934-.982}	.948 _{.898-.970}	.907 _{.742-.965}	.853 _{.658-.958}	.615 _{.343-.816}
		Ensemble	.965_{.936-.983}	.952_{.910-.972}	.933_{.799-.969}	.892_{.722-.967}	.672_{.442-.859}
	ASSD LV	Plain	0.77 _{0.47-1.15}	1.11 _{0.79-1.60}	1.58 _{0.90-3.53}	2.25 _{1.04-5.10}	6.81 _{2.63-14.20}
		BBB	0.76 _{0.45-1.14}	1.11 _{0.78-1.70}	2.20 _{0.95-5.68}	3.65 _{1.18-8.26}	9.84 _{4.27-21.04}
MCD-0.5		0.78 _{0.47-1.16}	1.05 _{0.76-1.51}	1.38 _{0.81-3.70}	2.10 _{0.92-5.72}	7.50 _{2.99-12.36}	
MCD-0.1		0.76 _{0.46-1.15}	1.08 _{0.77-1.56}	1.51 _{0.86-3.83}	2.35 _{1.00-5.76}	7.73 _{3.15-16.29}	
Ensemble		0.74_{0.43-1.12}	1.02_{0.72-1.46}	1.21_{0.75-2.91}	1.66_{0.82-4.62}	6.36_{1.89-11.22}	

Table 2: Probability calibration on images with increasing noise, blurring, or stretching distortions. Format: Median_{25th percentile}-75th percentile

		Degree of Distortion					
		0	1	2	3	4	
Noise	NLL ($\times 10^{-2}$)	Plain	0.94 _{0.66-1.32}	8.53 _{2.68-19.45}	20.37 _{7.63-38.49}	32.64 _{13.47-54.87}	47.85 _{19.72-73.98}
		BBB	0.95 _{0.67-1.31}	1.73 _{1.10-2.70}	2.35 _{1.33-4.08}	3.54 _{1.79-6.58}	8.52 _{3.81-15.41}
		MCD-0.5	0.97 _{0.69-1.35}	6.16 _{2.70-12.12}	11.13 _{4.86-20.18}	17.15 _{7.76-29.21}	29.91 _{13.40-45.40}
		MCD-0.1	0.94 _{0.67-1.32}	4.90 _{1.94-11.47}	12.67 _{4.72-23.80}	22.00 _{9.79-37.35}	38.16 _{16.56-59.05}
		Ensemble	0.92 _{0.65-1.28}	3.54 _{1.66-7.51}	7.40 _{2.98-15.80}	13.87 _{5.29-29.21}	32.59 _{12.42-55.13}
	Brier Score ($\times 10^{-3}$)	Plain	1.43 _{0.99-2.01}	6.64 _{2.92-12.52}	11.38 _{5.03-18.82}	14.97 _{6.60-22.88}	17.52 _{7.27-26.58}
		BBB	1.43 _{1.00-2.00}	2.55 _{1.62-4.00}	3.44 _{1.94-5.93}	5.04 _{2.51-9.03}	10.45 _{4.72-16.48}
		MCD-0.5	1.47 _{1.02-2.06}	7.53 _{3.42-13.17}	11.28 _{5.11-17.95}	14.38 _{6.43-21.71}	17.13 _{7.24-25.99}
		MCD-0.1	1.43 _{0.99-2.01}	5.77 _{2.57-10.48}	9.91 _{4.62-16.20}	13.46 _{6.28-21.03}	17.14 _{7.24-26.03}
		Ensemble	1.40 _{0.96-1.96}	4.99 _{2.30-10.45}	9.57 _{3.83-17.19}	13.90 _{5.78-21.92}	17.37 _{7.26-26.34}
Gaussian Blur	NLL ($\times 10^{-2}$)	Plain	0.94 _{0.66-1.32}	2.26 _{1.54-3.46}	4.77 _{2.60-8.96}	12.30 _{5.18-22.95}	24.51 _{9.26-41.24}
		BBB	0.95 _{0.67-1.31}	1.96 _{1.41-2.73}	3.47 _{2.21-5.28}	8.22 _{4.38-13.31}	17.92 _{8.53-28.82}
		MCD-0.5	0.97 _{0.69-1.35}	2.71 _{1.76-3.99}	5.59 _{2.89-9.69}	12.59 _{5.22-22.19}	21.42 _{8.84-35.15}
		MCD-0.1	0.94 _{0.67-1.32}	2.10 _{1.47-3.17}	4.11 _{2.39-7.36}	11.28 _{4.96-19.86}	23.53 _{9.88-37.88}
		Ensemble	0.92 _{0.65-1.28}	1.99 _{1.41-2.79}	3.37 _{2.17-5.03}	6.72 _{3.87-10.38}	13.36 _{6.71-21.80}
	Brier Score ($\times 10^{-3}$)	Plain	1.43 _{0.99-2.01}	3.27 _{2.19-4.85}	5.99 _{3.32-9.63}	11.43 _{5.18-17.25}	15.81 _{6.77-23.88}
		BBB	1.43 _{1.00-2.00}	2.86 _{2.01-4.02}	4.99 _{3.02-7.78}	10.59 _{5.08-16.29}	15.73 _{6.93-24.06}
		MCD-0.5	1.47 _{1.02-2.06}	3.92 _{2.46-5.98}	7.98 _{3.72-13.57}	13.96 _{5.62-21.96}	16.85 _{7.11-26.23}
		MCD-0.1	1.43 _{0.99-2.01}	3.07 _{2.08-4.63}	5.66 _{3.17-9.59}	11.97 _{5.26-18.55}	16.50 _{7.04-25.56}
		Ensemble	1.40 _{0.96-1.96}	2.88 _{1.99-4.12}	4.85 _{2.95-7.55}	9.80 _{4.85-14.91}	15.20 _{6.65-22.65}
Stretch	NLL ($\times 10^{-2}$)	Plain	0.94 _{0.66-1.32}	1.96 _{1.47-2.66}	3.34 _{1.95-5.73}	4.88 _{2.37-8.67}	13.35 _{6.05-19.84}
		BBB	0.95 _{0.67-1.31}	2.03 _{1.53-2.72}	3.74 _{2.19-5.97}	5.37 _{2.82-8.83}	12.42 _{6.07-18.46}
		MCD-0.5	0.97 _{0.69-1.35}	1.89 _{1.42-2.53}	2.90 _{1.90-4.72}	4.01 _{2.35-6.91}	9.97 _{5.07-14.89}
		MCD-0.1	0.94 _{0.67-1.32}	1.94 _{1.45-2.58}	3.09 _{1.92-5.02}	4.40 _{2.38-7.53}	11.38 _{5.57-16.73}
		Ensemble	0.92 _{0.65-1.28}	1.84 _{1.39-2.40}	2.73 _{1.76-4.11}	3.65 _{2.09-5.79}	8.66 _{4.32-12.76}
	Brier Score ($\times 10^{-3}$)	Plain	1.43 _{0.99-2.01}	2.86 _{2.17-3.76}	4.48 _{2.75-6.92}	6.10 _{3.26-9.35}	11.58 _{6.20-15.56}
		BBB	1.43 _{1.00-2.00}	2.96 _{2.23-3.97}	5.41 _{3.09-8.38}	7.58 _{3.90-11.45}	13.12 _{7.03-17.91}
		MCD-0.5	1.47 _{1.02-2.06}	2.77 _{2.10-3.69}	4.13 _{2.70-6.59}	5.62 _{3.29-9.01}	11.24 _{6.25-15.14}
		MCD-0.1	1.43 _{0.99-2.01}	2.82 _{2.15-3.71}	4.34 _{2.74-6.71}	5.97 _{3.31-9.18}	11.52 _{6.40-15.33}
		Ensemble	1.40 _{0.96-1.96}	2.70 _{2.05-3.50}	3.90 _{2.52-6.08}	5.26 _{2.94-8.34}	10.67 _{5.49-14.49}

Table 3: Predictive uncertainty measures on images with increasing noise, blurring, or stretching distortions. Format: Median_{25th percentile}-75th percentile

		Degree of Distortion					
		0	1	2	3	4	
Noise	Pred Entropy ($\times 10^{-2}$)	Plain	1.03 _{0.76-1.32}	1.10 _{0.29-1.72}	0.47 _{0.10-1.32}	0.13 _{0.04-0.60}	0.02 _{0.01-0.05}
		BBB	1.11 _{0.82-1.43}	1.66 _{0.99-2.34}	1.85 _{0.93-2.67}	1.95 _{0.72-2.91}	1.23 _{0.33-2.65}
		MCD-0.5	1.10 _{0.82-1.43}	2.13 _{1.12-3.09}	1.65 _{0.90-2.77}	1.11 _{0.69-1.96}	0.51 _{0.35-0.75}
		MCD-0.1	1.06 _{0.79-1.36}	1.50 _{0.49-2.18}	1.00 _{0.22-1.95}	0.40 _{0.11-1.31}	0.08 _{0.05-0.22}
		Ensemble	1.05 _{0.78-1.35}	1.74 _{0.42-3.05}	0.88 _{0.16-2.79}	0.22 _{0.05-1.35}	0.03 _{0.01-0.07}
	MI ($\times 10^{-3}$)	BBB	0.32 _{0.24-0.43}	1.26 _{0.65-2.46}	2.19 _{0.91-4.79}	3.54 _{1.12-7.38}	3.85 _{0.75-9.38}
		MCD-0.5	0.16 _{0.11-0.29}	4.32 _{2.18-6.96}	4.10 _{2.02-7.16}	2.82 _{1.56-5.75}	1.23 _{0.79-2.00}
		MCD-0.1	0.09 _{0.06-0.13}	1.68 _{0.44-3.54}	1.65 _{0.26-3.83}	0.74 _{0.14-2.92}	0.13 _{0.06-0.51}
		Ensemble	0.22 _{0.16-0.34}	5.42 _{1.06-14.00}	3.61 _{0.47-14.15}	0.82 _{0.14-7.07}	0.07 _{0.03-0.24}
	Dice _{WithinSamples} LV	BBB	.990 _{.984-.994}	.976 _{.920-.990}	.948 _{.804-.984}	.876 _{.699-.972}	.820 _{.656-.980}
		MCD-0.5	.994 _{.990-.997}	.856 _{.714-.964}	.835 _{.689-.956}	.892 _{.723-.976}	.984 _{.936-.996}
		MCD-0.1	.995 _{.992-.997}	.931 _{.836-.990}	.920 _{.813-.996}	.968 _{.838-1.00}	1.00 _{.988-1.00}
		Ensemble	.993 _{.987-.996}	.862 _{.672-.987}	.885 _{.670-1.00}	1.00 _{.800-1.00}	1.00 _{.00-1.00}
	ASSD _{WithinSamples} LV	BBB	0.21 _{0.17-0.27}	0.45 _{0.25-1.07}	0.86 _{0.32-2.65}	1.90 _{0.47-4.67}	2.96 _{0.17-6.60}
		MCD-0.5	0.12 _{0.08-0.16}	2.51 _{0.62-5.04}	2.94 _{0.57-5.92}	1.86 _{0.23-5.40}	0.17 _{0.00-1.07}
		MCD-0.1	0.10 _{0.07-0.14}	1.02 _{0.17-2.34}	1.16 _{0.00-2.75}	0.41 _{0.00-2.33}	0.00 _{0.00-0.10}
Ensemble		0.16 _{0.11-0.22}	3.34 _{0.26-7.43}	2.48 _{0.00-8.84}	0.00 _{0.00-4.48}	0.00 _{0.00-0.00}	
Gaussian Blur	Pred Entropy ($\times 10^{-2}$)	Plain	1.03 _{0.76-1.32}	2.01 _{1.27-2.58}	1.98 _{0.94-2.82}	1.34 _{0.33-2.29}	0.44 _{0.16-1.11}
		BBB	1.11 _{0.82-1.43}	2.28 _{1.43-3.02}	2.47 _{1.22-3.69}	1.71 _{0.47-3.07}	0.52 _{0.16-1.36}
		MCD-0.5	1.10 _{0.82-1.43}	2.52 _{1.44-3.62}	2.13 _{0.84-3.58}	1.04 _{0.33-2.16}	0.33 _{0.20-0.65}
		MCD-0.1	1.06 _{0.79-1.37}	2.09 _{1.35-2.69}	2.11 _{0.99-3.12}	1.29 _{0.30-2.40}	0.30 _{0.13-0.75}
		Ensemble	1.05 _{0.78-1.35}	2.31 _{1.42-3.11}	2.55 _{1.17-3.99}	1.90 _{0.44-3.75}	0.67 _{0.21-1.87}
	MI ($\times 10^{-3}$)	BBB	0.32 _{0.24-0.43}	1.64 _{0.83-2.90}	3.63 _{1.39-6.82}	3.71 _{1.07-8.27}	1.55 _{0.36-4.11}
		MCD-0.5	0.16 _{0.11-0.29}	3.10 _{1.34-5.50}	4.03 _{1.20-8.87}	2.39 _{0.57-5.93}	0.64 _{0.33-1.64}
		MCD-0.1	0.09 _{0.06-0.13}	0.81 _{0.37-1.66}	1.43 _{0.51-2.89}	1.09 _{0.26-2.68}	0.28 _{0.09-0.81}
		Ensemble	0.22 _{0.16-0.34}	2.55 _{1.09-5.37}	5.46 _{1.62-11.59}	5.13 _{0.92-14.59}	2.01 _{0.41-7.38}
	Dice _{WithinSamples} LV	BBB	.990 _{.984-.994}	.979 _{.958-.986}	.944 _{.840-.974}	.816 _{.688-.988}	.964 _{.804-1.00}
		MCD-0.5	.994 _{.990-.997}	.972 _{.891-.986}	.878 _{.708-.980}	.911 _{.732-1.00}	1.00 _{.972-1.00}
		MCD-0.1	.995 _{.992-.997}	.988 _{.968-.993}	.976 _{.898-.990}	.921 _{.788-1.00}	1.00 _{.956-1.00}
		Ensemble	.993 _{.987-.996}	.977 _{.928-.987}	.945 _{.822-.979}	.829 _{.610-1.00}	.900 _{.700-1.00}
	ASSD _{WithinSamples} LV	BBB	0.21 _{0.17-0.27}	0.40 _{0.31-0.73}	1.06 _{0.44-3.03}	3.40 _{0.19-6.34}	0.71 _{0.00-4.36}
		MCD-0.5	0.12 _{0.08-0.16}	0.54 _{0.26-1.99}	2.35 _{0.28-6.10}	1.79 _{0.00-5.77}	0.00 _{0.00-0.62}
		MCD-0.1	0.10 _{0.07-0.14}	0.22 _{0.16-0.47}	0.43 _{0.19-1.45}	1.10 _{0.00-2.99}	0.00 _{0.00-0.62}
Ensemble		0.16 _{0.11-0.22}	0.43 _{0.30-0.90}	0.92 _{0.40-4.67}	3.79 _{0.00-9.50}	0.78 _{0.00-6.59}	
Stretch	Pred Entropy ($\times 10^{-2}$)	Plain	1.03 _{0.76-1.32}	1.68 _{1.30-2.04}	1.87 _{1.04-2.30}	1.95 _{0.95-2.46}	1.30 _{0.60-2.11}
		BBB	1.11 _{0.82-1.43}	1.98 _{1.51-2.44}	2.39 _{1.21-3.06}	2.38 _{1.08-3.26}	1.46 _{0.70-2.39}
		MCD-0.5	1.10 _{0.82-1.43}	1.76 _{1.40-2.25}	2.19 _{1.30-2.82}	2.39 _{1.19-3.16}	1.72 _{0.77-2.91}
		MCD-0.1	1.06 _{0.79-1.37}	1.70 _{1.34-2.10}	2.01 _{1.14-2.55}	2.14 _{1.05-2.80}	1.50 _{0.65-2.49}
		Ensemble	1.05 _{0.78-1.35}	1.80 _{1.40-2.24}	2.17 _{1.25-2.86}	2.33 _{1.15-3.18}	1.71 _{0.75-2.95}
	MI ($\times 10^{-3}$)	BBB	0.32 _{0.24-0.43}	1.03 _{0.60-1.81}	2.48 _{1.02-4.88}	2.92 _{1.10-5.68}	2.25 _{0.80-4.71}
		MCD-0.5	0.16 _{0.11-0.29}	0.87 _{0.42-1.76}	2.57 _{1.02-5.18}	3.49 _{1.35-6.94}	3.64 _{1.14-7.55}
		MCD-0.1	0.09 _{0.06-0.13}	0.36 _{0.19-0.72}	1.10 _{0.40-2.21}	1.44 _{0.50-2.85}	1.44 _{0.43-3.20}
		Ensemble	0.23 _{0.16-0.34}	0.91 _{0.50-1.67}	2.50 _{1.01-5.22}	3.26 _{1.24-6.78}	3.62 _{1.19-7.93}
	Dice _{WithinSamples} LV	BBB	.990 _{.984-.994}	.983 _{.956-.993}	.937 _{.834-.982}	.922 _{.802-.970}	.865 _{.696-.950}
		MCD-0.5	.994 _{.990-.997}	.989 _{.965-.996}	.951 _{.864-.991}	.928 _{.838-.980}	.870 _{.724-.937}
		MCD-0.1	.995 _{.992-.997}	.992 _{.979-.997}	.971 _{.919-.995}	.960 _{.895-.989}	.918 _{.814-.968}
		Ensemble	.993 _{.987-.996}	.987 _{.968-.995}	.960 _{.900-.993}	.947 _{.877-.990}	.899 _{.737-.958}
	ASSD _{WithinSamples} LV	BBB	0.21 _{0.17-0.27}	0.33 _{0.19-0.63}	0.93 _{0.34-2.12}	1.18 _{0.47-2.53}	1.80 _{0.68-3.36}
		MCD-0.5	0.12 _{0.08-0.16}	0.20 _{0.10-0.50}	0.74 _{0.18-1.81}	1.12 _{0.33-2.21}	2.00 _{0.90-3.34}
		MCD-0.1	0.10 _{0.07-0.14}	0.16 _{0.09-0.31}	0.45 _{0.13-1.03}	0.64 _{0.19-1.30}	1.11 _{0.47-1.95}
Ensemble		0.16 _{0.11-0.22}	0.28 _{0.16-0.48}	0.62 _{0.20-1.37}	0.81 _{0.25-1.84}	1.58 _{0.56-3.92}	

Table 4: Segmentation accuracy and probability calibration metrics on the ACDC and UKBB datasets using model trained with UKBB dataset. Format: Median_{25th} percentile-75th percentile

	Pixelwise Accuracy \uparrow	Dice \uparrow			ASSD (mm) \downarrow			NLL \downarrow ($\times 10^{-2}$)	BS \downarrow ($\times 10^{-3}$)
		LV	Myo	RV	LV	Myo	RV		
UKBB \rightarrow UKBB									
Plain	.9960 _{.9944-9973}	.963 _{.932-981}	.899 _{.847-929}	.929 _{.850-964}	0.77 _{0.46-1.15}	0.82 _{0.58-1.12}	1.12 _{0.74-1.79}	0.94 _{0.66-1.32}	1.43 _{0.99-2.01}
BBB	.9960 _{.9944-9973}	.964 _{.934-982}	.899 _{.849-930}	.931 _{.853-966}	0.76 _{0.45-1.14}	0.82 _{0.57-1.12}	1.10 _{0.72-1.76}	0.95 _{0.67-1.31}	1.43 _{1.00-2.00}
MCD-0.1	.9960 _{.9944-9973}	.964 _{.934-982}	.899 _{.847-930}	.931 _{.850-965}	0.77 _{0.46-1.15}	0.82 _{0.58-1.12}	1.11 _{0.73-1.77}	0.94 _{0.67-1.31}	1.43 _{0.99-2.01}
MCD-0.5	.9959 _{.9942-9972}	.963 _{.933-981}	.896 _{.845-927}	.929 _{.847-964}	0.78 _{0.47-1.16}	0.84 _{0.60-1.15}	1.13 _{0.74-1.82}	0.97 _{0.69-1.35}	1.47 _{1.02-2.06}
Ensemble	.9961_{.9945-9974}	.965_{.936-983}	.902_{.852-933}	.935_{.863-967}	0.74_{0.43-1.13}	0.80_{0.55-1.10}	1.07_{0.69-1.71}	0.92_{0.65-1.28}	1.40_{0.97-1.96}
UKBB \rightarrow ACDC									
Plain	.9880 _{.9790-9923}	.927 _{.781-960}	.833 _{.728-871}	.870 _{.600-938}	1.40 _{1.00-2.94}	1.40 _{1.10-2.64}	1.86 _{1.09-5.96}	3.12 _{1.87-7.17}	4.39 _{2.77-8.05}
BBB	.9888 _{.9814-9927}	.938 _{.856-964}	.843 _{.769-876}	.884 _{.615-943}	1.27 _{0.93-2.12}	1.32 _{1.05-1.97}	1.64 _{1.03-4.84}	2.76 _{1.76-4.85}	4.03 _{2.64-6.81}
MCD-0.1	.9885 _{.9803-9927}	.935 _{.828-962}	.838 _{.754-873}	.879 _{.600-943}	1.33 _{0.95-2.36}	1.36 _{1.07-2.21}	1.69 _{1.05-5.27}	2.87 _{1.78-5.42}	4.15 _{2.67-7.22}
MCD-0.5	.9876 _{.9751-9923}	.930 _{.808-960}	.819 _{.669-866}	.862 _{.508-939}	1.39 _{0.99-2.55}	1.46 _{1.12-2.85}	1.91 _{1.09-6.96}	3.22 _{1.91-6.71}	4.53 _{2.79-9.06}
Ensemble	.9892_{.9822-9930}	.941_{.859-965}	.847_{.773-878}	.907_{.716-953}	1.23_{0.90-2.03}	1.28_{1.01-1.97}	1.41_{0.93-3.70}	2.71_{1.73-4.72}	3.94_{2.59-6.67}

Table 5: Predictive uncertainty measures on the ACDC and UKBB datasets using model trained with UKBB dataset. Format: Median_{25th} percentile-75th percentile

	Pred Entropy ($\times 10^{-2}$)	MI ($\times 10^{-3}$)	Dice _{WithinSamples}			ASSD _{WithinSamples}		
			LV	Myo	RV	LV	Myo	RV
UKBB \rightarrow UKBB								
Plain	1.03 _{0.77-1.33}	N/A	N/A	N/A	N/A	N/A	N/A	N/A
BBB	1.11 _{0.83-1.43}	0.32 _{0.24-0.43}	.990 _{.984-994}	.974 _{.964-0.979}	.982 _{.964-991}	0.214 _{0.167-0.273}	0.222 _{0.187-0.270}	0.286 _{0.200-0.432}
MCD-0.1	1.06 _{0.79-1.37}	0.09 _{0.06-0.13}	.995 _{.992-997}	.987 _{.982-0.989}	.991 _{.981-996}	0.099 _{0.071-0.137}	0.111 _{0.088-0.142}	0.142 _{0.091-0.238}
MCD-0.5	1.10 _{0.82-1.43}	0.16 _{0.11-0.29}	.994 _{.990-997}	.985 _{.979-0.988}	.988 _{.970-994}	0.116 _{0.083-0.162}	0.127 _{0.099-0.166}	0.188 _{0.117-0.372}
Ensemble	1.06 _{0.79-1.36}	0.22 _{0.16-0.34}	.993 _{.988-996}	.980 _{.971-0.985}	.985 _{.967-993}	0.159 _{0.113-0.219}	0.170 _{0.134-0.222}	0.245 _{0.155-0.404}
UKBB \rightarrow ACDC								
Plain	2.02 _{1.32-2.82}	N/A	N/A	N/A	N/A	N/A	N/A	N/A
BBB	2.35 _{1.55-3.55}	1.61 _{0.80-3.83}	.985 _{.964-991}	.961 _{.923-0.971}	.960 _{.840-984}	0.327 _{0.230-0.646}	0.353 _{0.254-0.668}	0.567 _{0.281-1.741}
MCD-0.1	2.15 _{1.42-3.18}	0.79 _{0.32-2.60}	.991 _{.974-995}	.975 _{.944-0.983}	.974 _{.876-991}	0.201 _{0.124-0.478}	0.231 _{0.146-0.514}	0.356 _{0.159-1.228}
MCD-0.5	2.53 _{1.60-4.15}	2.40 _{0.84-8.19}	.983 _{.925-993}	.956 _{.868-0.977}	.940 _{.755-984}	0.350 _{0.161-1.473}	0.396 _{0.192-1.549}	0.845 _{0.269-2.986}
Ensemble	2.30 _{1.50-3.63}	2.08 _{0.86-6.94}	.985 _{.948-992}	.957 _{.900-0.971}	.958 _{.814-986}	0.343 _{0.214-0.819}	0.390 _{0.242-0.938}	0.570 _{0.268-2.257}